https://doi.org/10.5194/acp-2019-1004
Preprint. Discussion started: 27 January 2020

Atmospheric Chemistry and Physics Discussions

Simulations of anthropogenic bromoform indicate high emissions at the coast of East Asia

Josefine Maas[1], Yue Jia[1], Birgit Quack[1], Jonathan V. Durgadoo[1], Arne Biastoch[1,2] and Susann Tegtmeier[1,*]

[1]GEOMAR Helmholtz Centre for Ocean Research Kiel, Kiel, Germany
[2]Kiel University, Kiel, Germany
*now at: Institute of Space and Atmospheric Studies, University of Saskatchewan, Saskatoon, Canada

Correspondence to: Josefine Maas (jmaas@geomar.de)

Abstract. Bromoform is the major by-product from chlorination of cooling water in coastal power plants. Power plants in East and Southeast Asian economies have increased rapidly exceeding global growth. Bottom-up estimates of bromoform emissions based on few measurements appear to under-represent the industrial sources of bromoform from East Asia. By means of Lagrangian analyses, we assess the amount of bromoform produced from power plant cooling water treatment in East and Southeast Asia. The spread of bromoform is simulated as passive particles that are advected using the 3-dimensional velocity fields from the high-resolution NEMO-ORCA0083 ocean general circulation model. Simulations are run for three scenarios with varying initial bromoform concentrations given by the range of measurements of bromoform in cooling water discharge. From comparison of our model results to observations, we expect initial bromoform concentrations between 20–60 µg L^{-1} used for the two lower scenarios, to be most realistic. From these two scenarios, we find elevated bromoform along the coastlines of East Asia with average concentrations of 23 and 68 pmol L^{-1} and maximum values in the Yellow, Japan and East China Seas. The industrially-produced bromoform is quickly emitted into the atmosphere with average air-sea flux of 3.1 and 9.1 nmol m^{-2} h^{-1}, respectively. Based on the emission estimates, atmospheric abundances of anthropogenic bromoform are derived from FLEXPART simulations and compared to simulations based on climatological bottom-up emission estimates. In the marine boundary layer of East Asia, anthropogenic bromoform amounts up to 0.5–1.6 ppt during boreal summer and is thus 2–7 times larger compared to the bottom-up estimates. During boreal winter some part of the anthropogenic bromoform is transported by the northeasterly winter monsoon towards the tropical regions, whereas during boreal summer anthropogenic bromoform is confined to the northern hemisphere subtropics. Convective events in the tropics entrain an additional 0.03 ppt of anthropogenic bromoform into the upper troposphere/lower stratosphere. We find that bromoform from cooling water treatment in East Asia is a significant source of atmospheric bromine responsible for annual emissions of 100–300 Mmol Br, which might be a missing factor in global flux estimates of organic bromine. About 90 % of this anthropogenic bromoform is discharged north of 20° N, while in the tropics natural sources dominate and only a small fraction of the anthropogenic bromoform reaches the stratosphere.

https://doi.org/10.5194/acp-2019-1004
Preprint. Discussion started: 27 January 2020

Atmospheric Chemistry and Physics Discussions

1 Introduction

Power plants require cooling water to regulate the temperature in the system. As their demand for cooling water is very high, power plants are often located at the coast to profit from an unlimited water supply. Seawater, however, needs to be disinfected to prevent biofouling and to control pathogens in effluents. The usual disinfection method, chlorination, is known to generate a broad suite of disinfection by-products (DBPs) including trihalomethanes, halogenated acetic acids and bromate (e.g. Helz et al., 1984; Jenner et al., 1997). DBPs develop when hypochlorous acid and organic matter react with the bromide and chloride ions contained in sea water (Allonier et al., 1999). Discharge of DBPs with the cooling water effluent can be harmful to the local ecosystem in combination with temperature and pressure gradients (Taylor, 2006). The composition and amount of generated DBPs depend on many factors including the type and concentration of the injected oxidant and the chemical characteristics of the treated water such as salinity, temperature and amount of dissolved organic matter (Liu et al., 2015). Cooling water effluents regularly discharge large volumes of water into the marine environment. This water is often warmer than the surrounding waters and decreases density at the sea surface. Chemicals such as DBPs contained in cooling water are likely to spread lateral across the sea surface which facilitates air-sea gas exchange for volatile DBPs.

One of the major DBPs is bromoform ($CHBr_3$), a halogenated volatile organic compound. Bromoform is also naturally produced in the ocean by macroalgae and phytoplankton and is the largest source of organic bromine to the atmosphere (Quack and Wallace, 2003). With an atmospheric lifetime of about 2–3 weeks, it belongs to the so-called very short-lived substances (VSLSs) (Engel and Rigby, 2018). Once bromoform is photolysed in the atmosphere, it can deplete ozone by catalytic cycles (Saiz-Lopez and von Glasow, 2012) or change the oxidising capacity of the atmosphere by shifting HO_x ratios towards OH (Sherwen et al., 2016). In the tropics, VSLSs such as bromoform can be entrained into the stratosphere through deep convection (e.g. Aschmann et al., 2009; Tegtmeier et al., 2015) and contribute to stratospheric ozone depletion (Hossaini et al., 2015). While the atmospheric abundance of chlorine and bromine species has started to decline as a result of the Montreal Protocol (Engel and Rigby, 2018), renewed productions and emissions of some long-lived ozone depleting substances (ODSs) have recently been discovered. The decline of CFC-11 has slowed unexpectedly, likely due to increasing emissions in eastern Asia (Montzka et al., 2018; Rigby et al., 2019). Atmospheric observations of carbon tetrachloride (CCl_4) also suggest ongoing anthropogenic emissions from feedstock and non-feedstock sources (Sherry et al., 2018). In contrast to the long-lived ODSs, emissions of halogenated VSLSs are not regulated by the Montreal Protocol, and their industrial contributions are not monitored. Current estimates of bromoform emissions suggest a global contribution to atmospheric bromine (Br) of 0.5–3.3 Gmol Br a^{-1} (Engel and Rigby, 2018). A bottom-up approach by Ziska et al. (2013) estimates 1.5 Gmol Br a^{-1}. Their analysis is based on the HalOcAt (Halocarbons in the Ocean and Atmosphere) database (https://halocat.geomar.de/) which contains VSLSs data in surface ocean and atmosphere from measurement campaigns. Based on physical and biogeochemical characteristics of the ocean and atmosphere, the data are classified into 21 regions and extrapolated to a regular grid within each region. Top-down bromoform emission estimates, on the other hand, are based on global model simulations adjusted to match available aircraft observations. They are in general, a factor of two larger than bottom-up emission estimates. Individual ship cruises, aircraft

https://doi.org/10.5194/acp-2019-1004
Preprint. Discussion started: 27 January 2020

Atmospheric Chemistry and Physics Discussions

campaigns and modelling studies have demonstrated a large spatio-temporal variability of bromoform in surface water and air (e.g. Fiehn et al., 2017; Fuhlbrügge et al., 2016; Jia et al., 2019). These pronounced variations combined with the poor temporal and spatial data coverage is a major challenge for deriving reliable emission estimates and may explain the large deviations between bottom-up and top-down estimates. Geographical regions with poor data coverage might not be well represented in the global emission scenarios. Furthermore, the anthropogenic input of bromoform might be under-estimated for large industrial regions (Boudjellaba et al., 2016).

Industrially produced bromoform will spread in the marine environment once the treated water is released and will be emitted into the atmosphere together with naturally produced bromoform. Atmospheric and oceanic measurements cannot distinguish between naturally and industrially produced bromoform and all top-down and bottom-up emission estimates discussed above automatically include the latter. A first comparison of natural and industrial bromoform sources from Quack and Wallace (2003) concluded a negligible global contribution of 3 % man-made bromoform. Their estimate was based on measurements of bromoform in disinfected water (80 nmol L^{-1}) from European power plants and cooling water use and projections of the global electricity production. In the meantime, the global electricity production has increased by almost 50 % from 16700 TWh in 2003 (IEA, 2005) to 25000 TWh in 2016 (IEA, 2018). Furthermore, new measurements of bromoform in disinfected cooling water have become available suggesting potentially higher concentrations of up to 500 nmol L^{-1} (Yang, 2001). Especially emerging economies in East Asia, such as China have experienced a massive growth over the last years exceeding the global economic growth. As the existing estimate of industrially produced bromoform is outdated, updated estimates taking into account new measurements are required to assess the impact of anthropogenic activities on the production and release of brominated VSLSs as well as their contribution to stratospheric ozone depletion.

We aim to quantify anthropogenic contributions to VSLSs, in form of bromoform emitted from regional industrial activities. As 50 % of global coastal cooling water is produced in East and Southeast Asia, we define these areas as our study region. We identify locations of high industrial activity along the coast of East and Southeast Asia and derive estimates of released cooling water and therein contained bromoform (Section 2). Based on Lagrangian simulations in the ocean, we derive the general marine distribution of non-volatile DBPs released with cooling water. For the case study of bromoform, we show oceanic distribution of the volatile DBP by taking air-sea exchange into account (Section 3). Based on the oceanic emissions, the atmospheric distribution of bromoform generated in industrial cooling water is simulated with a Lagrangian particle dispersion model (Section 4). Results are compared to existing observational atmospheric and oceanic distributions (Section 5). Methods are described in Section 2, while discussion and summary are provided in Section 6.

https://doi.org/10.5194/acp-2019-1004
Preprint. Discussion started: 27 January 2020

Atmospheric Chemistry and Physics Discussions

2 Methods

2.1 DBP production in cooling water from global power plants

In this study, we investigate the oceanic distribution of DBPs produced in power plants that chlorinate seawater. We assume that all power plants located at the coast use seawater for cooling purposes. Most of the seawater is only used once in the system as the ocean provides unlimited water supply. For the estimation of the cooling water volumes, we use the global power plant database Enipedia (enipedia.tudelft.nl, last access: 2017) where over 21,000 power plants are given together with location, electricity generation (in MWh) and sometimes fuel type. Based on the coordinates, we choose those power plants that are located less than 0.02 degrees (maximum 2 km at the equator) away from any coastline and refer to them as coastal. Based on this classification, 23 % of energy capacity from listed power plants in the database is generated by coastal power plants. The Key World Energy Statistics (IEA, 2018) give a total global electricity production of 24973 TWh in 2016. The average water use per MWh energy was given by Taylor (2006) to be 144 m^3 MWh^{-1} which leads to a global cooling water discharge of about 800 billion m^3 a^{-1} along the coast in 2016. For the individual coastal power plants in East and Southeast Asia, annual cooling water volumes are shown in Figure 1.

To determine the amount of bromoform produced in the cooling water, there are only a few measurements available and the locations are limited (Table 1). Most data originate from several power plants in Europe (Allonier et al., 1999; Boudjellaba et al., 2016; Jenner et al., 1997) and some studies are based on measurements from single power plants in Asia (Padhi et al., 2012; Rajamohan et al., 2007; Yang, 2001). Furthermore, the location where water is sampled is not consistent among the different studies. Some samples were taken in the coastal surface water at the power plant outlet (Fogelqvist and Krysell, 1991; Yang, 2001), while other studies sampled directly inside the power plant before dilution with the ocean (Jenner et al., 1997; Rajamohan et al., 2007). The measurements show a very large variability ranging from 8–290 µg L^{-1}. As there is no systematic difference between measurements inside the power plant and at the power plant outlet, both types of measurements are given in Table 1 together in column 1.

In addition to the sampling location, differences in the concentrations can result from water temperature, salinity and dissolved organic carbon content, which are seasonally dependent. Colder water from mid- to high latitudes during winter requires less water treatment as the settlement of pathogens takes longer compared to tropical or subtropical waters. The chlorination dosage and frequency of treatment also play a distinct role for the resulting DBP concentrations (Joint Research Council, 2001).

Given that available measurements are sparse and depend on many factors, the uncertainties in initial bromoform concentrations in cooling water are relatively high. For our analyses we chose to scale the bromoform discharge according to three scenarios (LOW, MODERATE and HIGH), which reflect the range of values given in available literature (Table 1). For our simulations, we use initial bromoform concentrations of 20 µg L^{-1} (LOW), 60 µg L^{-1} (MODERATE) and 100 µg L^{-1} (HIGH) in undiluted cooling water.

https://doi.org/10.5194/acp-2019-1004
Preprint. Discussion started: 27 January 2020

Atmospheric Chemistry and Physics Discussions

2.2 Lagrangian simulations in the ocean

For the assessment of the long-term, large-scale effect of DBPs from power plant cooling water on the environment, we simulate the distribution of non-volatile DBPs and the concentration and emission of the volatile DBP bromoform in the ocean. The Lagrangian model runs are based on velocity output from the high-resolution, eddy-rich ocean general circulation model (OGCM) NEMO-ORCA version 3.6 (Madec, 2008). The ORCA0083 configuration (The DRAKKAR Group, 2007) has a horizontal resolution of 1/12 degrees at 75 vertical levels and output is given at a temporal resolution of five days for the time period 1963–2012. Atmospheric forcing comes from the DFS5.2 data set (Dussin et al., 2016). The experiment ORCA0083-N06 used in this study was run by the National Oceanography Centre, Southampton, UK. Further details can be found in Moat et al. (2016).

We simulate the spread of the DBPs from treated cooling water, by applying a Lagrangian trajectory integration scheme to the 3D velocity fields with the ARIANE software (Blanke et al., 1999). We perform offline trajectory calculations by passively advecting virtual particles which represent the DBP amount discharged with the cooling water. The calculation of trajectories is purely advective without diffusivity. For each scenario we perform one simulation over the same time period. In each simulation, particles are continuously released close to the power plant locations at 5-day time steps over two years. We allow for an accumulation period of 11 months and show the results of the seasonal and annual mean of the second year starting in December. A detailed description of the applied method can be found in Maas et al., (2019) where it is also shown that interannual variability of surface velocity in the study region is small compared to seasonal variability.

Our study focusses on the region of East and Southeast Asia (90° E–165° E, 10° S–45° N), which comprises 50 % of the global coastal power plant capacity and cooling water discharge. The particle discharge locations have been chosen as close to the coastlines as possible (Figure 2). Particles are released approximately 8 to 40 km offshore, as the model-resolution does not allow to capture smaller-scale coastal structures such as harbours or estuaries nor does it simulate the near-costal exchange, e.g. through tides. Our approach ensures minimal influence of the land boundaries on the simulation in order to avoid numerically-related beaching of particles into the coastal boundary.

For the analysis of the experiments we distinguish 1) the passive spread of DBPs without any environmental sinks, and 2) the spread of bromoform as a major volatile DBP accounting for atmospheric fluxes and oceanic sinks. For the passive spread of non-volatile DBPs, we consider the full history of simulated particle positions which is equivalent to assuming no particles getting lost through sinks in the ocean or emission into the atmosphere. The resulting distribution shows locations where non-volatile DBPs such as bromoacetic acid are transported through the ocean currents within one year. For the spread of anthropogenic bromoform, each particle is assigned an initial mass of bromoform according to the amount of cooling water used by the respective power plant (Figure 1) and the bromoform concentration prescribed by the three scenarios, MODERATE,

https://doi.org/10.5194/acp-2019-1004
Preprint. Discussion started: 27 January 2020

Atmospheric Chemistry and Physics Discussions

HIGH and LOW. The particle density distribution is calculated at the sea surface down to 20 m on a 1°×1° grid. The distribution is given as particle density per grid box in percent for non-volatile DBPs and as concentration in pmol L^{-1} for bromoform.

Sink processes of bromoform such as constant gas exchange at the air-sea interface or chemical loss rates are taken into account. The air-sea flux of bromoform is calculated after the general flux equation at the air-sea interface:

$$Flux = (C_w - C_{eq}) \cdot k \quad (1)$$

Here Flux is positive when it is directed from the ocean to the atmosphere and is given in pmol m^{-2} h^{-1}. C_w is the actual concentration in the surface mixed layer in pmol L^{-1} and C_{eq} is the theoretical equilibrium concentration at the sea surface (in pmol L^{-1}) calculated from the atmospheric mixing ratio (in ppt), sea surface temperature and sea surface salinity (Quack and Wallace, 2003). The gas transfer velocity k (in cm h^{-1}) mainly depends on the surface wind speed and temperature and is calculated after Nightingale et al., (2000). Wind velocities at 10 m height are taken from the NEMO-ORCA forcing data set DFS5.2 (Dussin et al., 2016) which is based on the ERA-interim atmospheric data product.

As the oceanic and atmospheric terms in the air-sea flux parameterisation are of additive nature, it is possible to calculate the flux of anthropogenic and natural bromoform separately. For our simulations, we only consider bromoform from cooling water and apply the air-sea flux parameterisation to the anthropogenic portion of bromoform in water and air. We have conducted sensitivity tests (see section 2.3) to estimate the impact of atmospheric bromoform abundances on the flux calculations. The tests show that outgassed anthropogenic bromoform leads to atmospheric surface values C_{eq}, which are always below 8 % of the underlying sea surface concentration C_w (at a water temperature of 20°C). Such low equilibrium concentrations can be considered negligible for the flux calculation and therefore C_{eq} is set to zero in our study.

The sea surface concentration and air-sea flux from the three simulations are also compared to climatological maps of bromoform concentration and emissions from the updated Ziska et al. (2013) inventory (hereafter referred to as Ziska2013) (Fiehn et al., 2018).

Mean concentrations are calculated by averaging over the area where 90 % of bromoform, characterised by the highest local concentrations, accumulate. Maximum concentrations are calculated by averaging over the area where 10 % of the highest bromoform values accumulate. Mean and maximum fluxes are calculated based on the same principle. The annual mean atmospheric bromine input from industrial bromoform emissions in East and Southeast Asia is derived from the air-sea flux maps of the whole domain.

2.3 Lagrangian simulation in the atmosphere

Based on the seasonal mean emission maps, we obtain a source function of atmospheric bromoform. We simulate the atmospheric transport and distribution of bromoform for the three scenarios with the Lagrangian particle dispersion model FLEXPART

https://doi.org/10.5194/acp-2019-1004
Preprint. Discussion started: 27 January 2020

Atmospheric Chemistry and Physics Discussions

(Stohl et al., 2005). Bromoform emissions derived from the three scenarios are used as input data at the air-sea interface over the East and Southeast Asia area defined as our study region. The meteorological input data (temperature, wind) stem from the ERA-Interim reanalysis (Dee et al., 2011) and are given on a 1°×1° horizontal grid, at 61 vertical model levels and a 3-hourly temporal resolution. The chemical decay of bromoform in the atmosphere was accounted for by prescribing a half-life of 17 days during all runs (Montzka and Reimann, 2010). Output mixing ratios are given at the same horizontal resolution and 33 vertical levels from 50 to 20000 m. Detailed descriptions of model settings are described in Jia et al. (2019). The FLEXPART simulations were performed for the boreal winter (December–February, DJF) and summer (June–August, JJA) seasons, respectively, for a total of three months with a one-month spin-up.

We perform three additional FLEXPART runs based on the updated Ziska2013 emission inventory with the same FLEXPART configuration as described above for both seasons, DJF and JJA. As the Ziska2013 inventory currently presents our best knowledge of bottom-up derived bromoform emissions, it is of interest to analyse how much of these emissions can be explained by industrial sources and how much stems from natural sources.

The first run uses only the Ziska2013 emissions over the East and Southeast Asia area defined as our study region. This run is named Ziska2013-EastAsia and is used to compare the resulting mixing ratios in the atmospheric boundary layer to results driven by our anthropogenic emissions in the East and Southeast Asia region.

For comparisons of mixing ratios in the free troposphere and upper troposphere/lower stratosphere (UTLS) approximately above 17 km, emissions from other parts of the tropics also need to be taken into account as the time scales for horizontal transport are often shorter than the ones for vertical transport. Therefore, we set up two additional runs using the Ziska2013 emissions for the global tropics and subtropics between 45° S and 45° N. This configuration is used as input for the first of the two runs, which is named Ziska2013-Tropics.

As the Ziska2013 emissions are based on extrapolation of very few northern hemispheric coastal data, it likely neglects anthropogenic emissions in some regions. Therefore, the second run, Ziska2013-Mixed, uses the same Ziska2013 emissions between 45° S and 45° N, except for the East and Southeast Asia region. Here, the Ziska2013 emissions are replaced by the MODERATE emission values for every grid box where the MODERATE emissions are larger than Ziska2013. These two runs, Ziska2013-Mixed and Ziska2013-Tropics, are used to compare additional anthropogenic bromoform based on the MODERATE scenario to bromoform based on the Ziska2013 climatology for the UTLS region.

Mean mixing ratios from the whole domain in the marine boundary layer and in the UTLS are given as the average over the 90 % area characterised by the highest local values, and maximum mixing ratios as the average over the largest 10 % (see Section 2.2). In a second step, we identify two regions in order to analyse the vertical transport of bromoform into the free troposphere and into the UTLS. For the height profiles of the Ziska-Tropics and the Ziska-Mixed runs, we average mixing ratios over a region

https://doi.org/10.5194/acp-2019-1004
Preprint. Discussion started: 27 January 2020

above the maritime continent which we refer to as the tropical box (10° S–20° N, 90° E–120° E), and another region from China to Japan which we refer to as the subtropical box (30° N–40° N, 120° E–145° E) (Figure 2).

3 Oceanic spread of DBPs and bromoform

The particle density distribution shows the annual mean DBP accumulation pattern in the research area of interest (Figure 3). Non-volatile DBPs from cooling water usually accumulate around the coast and in the marginal seas. There is a clear latitudinal gradient with only little DBP distribution south of 20° N, except for higher values in the Strait of Malacca. In contrast to the relatively low DBP density in the inner tropics, the subtropics show a very high accumulation of DPBs with a centre in the marginal seas between 25° N and 40° N. While power plants can be found along all coastlines (Figure 1), the power plant capacity and therefore the amount of treated cooling water is much higher along the subtropical coasts of China, Korea and Japan leading to the DBP distribution pattern shown in Figure 3. Hot spots are around the coast of Shanghai and Incheon with a DBP density of 1 %. A relatively high DBP density of 0.8 % can also be found in the East China Sea, the Yellow Sea, the southern Japan Sea, the Gulf of Tonkin and the Strait of Malacca. Medium to low DBP density in the South China Sea suggest only small contributions of cooling waters to this region. Since Japan and Korea have a large number of power plants with high volumes of cooling water discharge, a relatively large amount of DBPs is transported with the Kuroshio Current into the North Pacific.

The distribution of bromoform, as a volatile DBPs in the surface ocean differs from the DBP accumulation pattern shown in Figure 3, as the volatile DBPs are outgassed into the atmosphere. The annual mean sea surface concentration of bromoform from cooling water is shown in Figure 4 (panel a-c) for the three scenarios LOW, MODERATE and HIGH and with a substantially smaller spread compared to non-volatile DBPs. The area which contains the 90 % highest bromoform concentrations does not vary between the three scenarios, as the air-sea flux, which determines how much bromoform remains in the water, is linearly proportional to the sea surface concentration. Higher surface concentrations result in higher fluxes into the atmosphere, which limits the spread of bromoform substantially compared to non-volatile DBPs. Bromoform concentrations are around 23, 68, and 113 pmol L^{-1} (LOW, MODERATE and HIGH) averaged over the region where the 90 % of bromoform with the highest concentrations accumulate (Table 2). This region is to a large degree limited to latitudes north of 20° N as a result of the power plant distribution. As in the case of the non-volatile DBPs, most of the bromoform is centred along the Chinese, Korean and Japanese coast line with a larger spread into the marginal seas for the latter two. One exception to this latitudinal gradient is the Strait of Malacca where local power plants result in average bromoform concentrations of 3.4, 10.3 and 16.7 pmol L^{-1} (LOW, MODERATE, and HIGH).

Observational based oceanic bromoform concentrations from Ziska2013 (Figure 4, panel d) are relatively evenly spread along the coastlines of the region and do not show the latitudinal gradient found for the anthropogenic concentrations. North of 20° N the anthropogenic bromoform is much higher than the oceanic distribution from Ziska2013, where the maximum lies around 21 pmol L^{-1}. Our simulations reach maximum values (averaged over the 10 % highest bromoform concentrations) of 112, 338

https://doi.org/10.5194/acp-2019-1004
Preprint. Discussion started: 27 January 2020

and up to 563 pmol L^{-1} (LOW, MODERATE and HIGH, Table 2) in the Japan Sea. These concentrations are all above 100 pmol L^{-1} and are very high compared to observational values from Ziska2013 (Figure 4, panel d).

Emissions of anthropogenic bromoform show a similar distribution as the oceanic concentrations (Figure 5, panel a-c). Flux rates averaged over the region of the 90 % highest flux values are 3, 9 and 15 nmol m^{-2} h^{-1} (LOW, MODERATE and HIGH). Maximum flux rates (averaged over the highest 10 %) even reach 13, 41 and 68 nmol m^{-2} h^{-1} in the Japan Sea near the Korean and Japanese coast for the three scenarios (Table 2). In contrast, the existing observational based estimates from the Ziska2013 climatology peak with 1.1 nmol m^{-2} h^{-1} located in the South China Sea along the west coast of the Philippines (Figure 5, panel d).

The annual bromine input from bromoform into the atmosphere in the East and Southeast Asia region is 118 Mmol according to the observation-based inventories from Ziska2013 (Table 2). Our simulations suggest that the anthropogenic input alone amounts to 100, 300 and 500 Mmol Br a^{-1} (LOW, MODERATE, HIGH) for the same region, which is almost 99 % of the bromine produced as bromoform during cooling water treatment in the power plant. While average and maximum emissions are much higher for anthropogenic bromoform as discussed above, the Ziska emissions spread out over a larger area thus resulting in similar total emissions as the LOW scenario. 90 % of the atmospheric bromine input from anthropogenic bromoform occurs north of 20° N where 89–447 Mmol Br are released over one year, compared to the regions south of 20° N where only 10–52 Mmol Br a^{-1} enter the atmosphere (from LOW to HIGH). In contrast, only 29 % of bromine is released into the atmosphere north of 20° N for the Ziska2013 climatology.

4 Anthropogenic bromoform in the atmosphere

4.1 Mixing ratios in the marine boundary layer

Atmospheric mixing ratios of anthropogenic bromoform are derived from FLEXPART runs driven by the seasonal emission estimates discussed in section 3. Atmospheric bromoform from industrial emissions is shown for a 5-day average at 50 m height for JJA for all three scenarios (Figure 6, panel a-c). Mean mixing ratios are 0.5, 1.6 and 2.4 ppt (LOW, MODERATE, HIGH, Table 2). Overall, high atmospheric mixing ratios are found around the coastlines of Japan, South Korea and northern China. Although maximum emissions are located in the Japan Sea, maximum mixing ratios are mostly located south of Japan with values up to 4.6, 13.9 and 23.3 ppt (LOW, MODERATE, HIGH, Table 2). Here, the westerlies lead to bromoform transport from the Japan Sea into the Northwest Pacific. We also localise hot spots of strong anthropogenic bromoform accumulations due to enhanced emissions over Shanghai, Singapore or the Pearl River Delta, respectively (Figure 6, panel a). During boreal summer, the West Pacific and Maritime Continent are influenced by southwesterly winds and the anthropogenic bromoform experiences northward transport, bringing some smaller portion of the subtropical emissions into the mid-latitudes (Figure 6, panel a, b and c).

https://doi.org/10.5194/acp-2019-1004
Preprint. Discussion started: 27 January 2020

Atmospheric Chemistry and Physics Discussions

During boreal winter (DJF, Figure 7, panel a-c), anthropogenic bromoform shows somewhat lower atmospheric mixing ratios with a mean of 0.3, 0.9 and 1.5 ppt and maximum values of 3.2, 9.5 and 15.9 ppt for the three scenarios (Table 2). In contrast to boreal summer, the atmospheric transport is dominated by winds from the northeast and higher bromoform values are confined to tropical and subtropical regions (Figure 7). Thus, tropical mixing ratios show a clear seasonal variability and are on average over 3 times higher for DJF than for JJA without large shifts in the location of the bromoform emissions (Figure S1).

In order to compare the atmospheric impact of industrial emissions with existing results, we repeat our analysis for the bottom-up emissions scenario Ziska2013 for the same region, which has been frequently used in past studies (e.g. Hossaini et al., 2013, 2016). Atmospheric mixing ratios are derived from seasonal FLEXPART runs driven by Ziska2013-EastAsia and shown for a 5-day average at 50 m height for JJA (Figure 6d). For both seasons, atmospheric bromoform based on industrial emissions is larger than atmospheric bromoform based on the Ziska2013 emissions. These differences maximise in the subtropical regions, where anthropogenic bromoform dominates especially during JJA when anthropogenic mixing ratios are 2–7 times larger than from climatological emissions (for LOW and MODERATE). In the tropical regions, the situation is more complicated. Atmospheric abundances driven by the industrial emissions reach higher peak values of up to 2 ppt especially in the Strait of Malacca (MODERATE, Figure 6b) while mixing ratios driven by the observationally based emissions from Ziska2013-EastAsia are smaller only reaching peak values of up to 0.8 ppt, but are spread over a much wider area (Figure 6d). Given the comparison of the boundary layer values, it is not clear which emission scenario will result in a larger contribution to stratospheric halogen budget.

4.2 Vertical transport of bromoform in the troposphere

In order to analyse atmospheric transport from the marine boundary layer into the free troposphere and UTLS, bromoform mixing rations are averaged over a subtropical box (30° N–40° N, 120° E–145° E, Figure 2) and a tropical box (10° S–20° N, 90° E–120° E, Figure 2) from the Ziska2013-Tropics and Ziska2013-Mixed simulations for DJF and JJA. Both simulations are based on global climatological Ziska2013 emissions between 45° S and 45° N, with Ziska2013-Mixed including additional anthropogenic bromoform emissions in East and Southeast Asia.

In the subtropical box (Figure 8), there is a strong dominance of anthropogenic bromoform in the marine boundary layer during JJA several times higher compared to bromoform of climatological bottom-up emissions (Figure 8). Our simulations suggest that during convective events in JJA, anthropogenic bromoform from the subtropical marine boundary layer can be transported into the UTLS region up to 17 km, the approximate height of the cold point. In our example, convective events occur during the second half of the summer bringing occasionally higher bromoform of over 0.3 ppt into the UTLS (Figure 8a).

During DJF (Figure S2), there is only very little transport of bromoform out of the boundary layer, and entrainment of anthropogenic bromoform into the subtropical UTLS is confined to boreal summer when the intertropical convergence zone (ITCZ) is located north of 10° N (Waliser and Gautier, 1993).

https://doi.org/10.5194/acp-2019-1004
Preprint. Discussion started: 27 January 2020

In the tropical box, atmospheric bromoform mixing ratios in the marine boundary layer are weaker than in the subtropics for the simulation based on Ziska2013-Mixed emissions (Figure 9, panel a and b). However, the vertical transport for the two simulations Ziska2013-Mixed and Ziska2013-Tropics are in the same range from 0.2–0.5 ppt (Figure 9) even though the spatial distribution of emissions between Ziska2013 and the MODERATE scenario differs strongly (Figure 5). The seasonal difference between DJF and JJA is very pronounced in the marine boundary layer where tropical mixing ratios during DJF exceed 0.5 ppt throughout the whole time period (Figure 9a). Thus, convective events during DJF bring more bromoform into the UTLS compared to JJA, especially for the run Ziska2013-Mixed which include the anthropogenic bromoform emissions (Figure 9). While the air-sea fluxes in the tropics hardly change from DJF to JJA (Figure S1), the prevailing northeasterly winds during DJF advect the bromoform from the high emissions in East Asia towards the maritime continent which increases tropical abundances substantially. This can be seen for Ziska2013 and even stronger in the MODERATE run where the East Asian emissions dominate over the Southeast Asian region (Figure 7, panel b and d).

4.3 Mixing ratios in the upper troposphere/lower stratosphere

Atmospheric processes over the maritime continent, which encloses the tropical box, are characterised by deep convective events which can lead to entrainment of VSLS into the stratosphere (Aschmann and Sinnhuber, 2013; Tegtmeier et al., 2019). For our case study, convective events reaching the UTLS occur frequently in both seasons sometimes persisting over several days (Figure 9). There is a clear anthropogenic signal in the free troposphere in both seasons, which is more pronounced during DJF (Figure 9a) than during JJA (Figure 9b) in agreement with the elevated mixing ratios in the marine boundary layer.

In addition to the mixing ratios averaged over two boxes, we show the spatial distribution of bromoform at 17 km for the whole domain as a 5-day snapshot (Figure 10) based on the bottom-up Ziska emissions only (Ziska2013-Tropics), and emissions estimates taking anthropogenic sources into account (Ziska2013-Mixed). During DJF (Figure 10, panel a and c), there is a clear anthropogenic signal over the Bay of Bengal, across the equator towards Indonesia. Mixing ratios for the Ziska2013-Mixed run are 0.19 ppt averaged over the area of 90 % highest mixing ratios and 0.16 ppt for Ziska2013-Tropics, corresponding to 0.03 ppt being of anthropogenic origin (Table S1). Again, the stronger advective transport in the boundary layer during DJF bringing higher bromoform abundances from the subtropics into the tropics plays an important role here. As a result more bromoform is picked up by convection and transported into the UTLS during DJF than during JJA. Bromoform mixing ratios are slightly smaller during JJA, with 0.17 ppt and 0.15 ppt based on the Ziska2013-Mixed and Ziska2013-Tropics emissions, respectively (Table S1). Here, more anthropogenic bromoform stays in the northern hemisphere and convection is confined to few areas in the Bay of Bengal and Thailand (Figure 10, panel b and d). Although over 90 % of anthropogenic bromoform is outgassed north of 20° N, we find that these emissions contribute 0.02–0.03 ppt to the stratospheric bromine budget which is an increase of 14–19 % in the MODERATE scenario compared to the Ziska2013 climatology.

https://doi.org/10.5194/acp-2019-1004
Preprint. Discussion started: 27 January 2020

Atmospheric Chemistry and Physics Discussions

5 Comparison with observations

5.1 Bromoform measurements in the ocean

Observations in the surface ocean and atmosphere from East and Southeast Asia can help to determine which scenario (LOW, MODERATE, HIGH) offers the best fit for simulating anthropogenic bromoform in this region. Recent measurement campaigns show elevated bromoform concentrations in the coastal waters of the East China and Yellow Seas (He et al., 2013a, 2013b; Yang et al., 2014, Yang et al., 2015). Average values of 6–13 pmol L^{-1} were measured in the Yellow and East China Seas during boreal spring and summer (Yang et al., 2014; Yang et al., 2015), and of 17 pmol L^{-1} were measured in boreal winter (He et al., 2013b). Particularly high concentrations were detected by He et al. (2013a) during spring in the East China Sea with a mean of 134 pmol L^{-1}. Highest bromoform concentration over 34 pmol L^{-1} (He et al., 2013b) and over 200 pmol L^{-1} He et al. (2013a) were observed near the estuaries of the Yangtse River, which the authors attributed to anthropogenic activities including coastal water treatment in the Shanghai region. Our simulations also show mean surface concentrations around Shanghai of 14–71 pmol L^{-1} (LOW to HIGH), in the range of the observations by He et al. (2013a).

Measurements in the South China and Sulu Seas (Fuhlbrügge et al., 2016) show a high variability of bromoform in the surface seawater with average concentrations of 19.9 pmol L^{-1}. Highest values of up to 136.9 pmol L^{-1} are found close to the Malaysian Peninsula and especially in the Singapore Strait suggesting industrial contributions. Maximum anthropogenic bromoform from our simulations in the Singapore Strait ranges from 36–178 (LOW to HIGH), in good agreement with maximum values reported by Fuhlbrügge et al., (2016).

Average anthropogenic bromoform concentrations for the three scenarios are around 23–113 pmol L^{-1} (averaged over the region of the 90 % highest values, Table 2) and are larger than the observational average values. The larger model values might be due to the fact that the cooling water effluents do not distribute far into the marginal seas but stay near the coast as observed by Yang (2001) and confirmed by our simulations. Our simulated anthropogenic bromoform concentrations stay usually within 100 km of the coast, the averaged observational values, however, include also measurements that are up 200 km away from the coastline and can therefore be expected to be lower. While observational mean values are slightly lower than the model results, maximum values found close to the coast line show very good agreement with the model results.

5.2 Bromoform measurements in the marine boundary layer

Atmospheric mixing ratios are 0.9 ppt and 0.3 ppt in the subtropical East China Sea during boreal winter and summer, respectively (Yokouchi et al., 2017). Our simulations in the East China Sea suggest anthropogenic bromoform contributions of 1.7–5.1 ppt near Shanghai, being on the upper side of the observations. Nadzir et al. (2014) observed relatively high values in the South China Sea (1.5 ppt) and the Strait of Malacca (3.7 ppt) during boreal summer. Our simulations show average mixing ratios of 0.5–1.8 ppt at the surface (LOW to MODERATE) near the Pearl River Delta in the South China Sea, in good agreement

https://doi.org/10.5194/acp-2019-1004
Preprint. Discussion started: 27 January 2020

with Nadzir et al. (2014). In the Strait of Malacca, our simulations suggest 0.2–0.7 ppt (LOW to MODERATE) which is lower than the observations.

Further south in the South China and Sulu Seas, Fuhlbrügge et al. (2016) measured atmospheric bromoform mixing ratios of 2 ppt during November. Near Singapore, the authors reported 3.4 ppt consistent with the high oceanic concentrations observed in the same region. Our simulations result in peak mixing ratios around Singapore during DJF of up to 1.7 and 5.3 ppt for the LOW and MODERATE scenario, respectively, in good agreement with Fuhlbrügge et al. (2016). Especially the high atmospheric bromoform mixing ratios found near Singapore and the Pearl River Delta can be associated with anthropogenic activity.

The HIGH scenario shows average mixing ratios which are in general too high for the whole domain. Thus, it is not likely that cooling water treatment produces anthropogenic bromoform with average concentrations of 100 µg L^{-1}. Nevertheless, such concentrations can occur at some locations and produce extremely high bromoform abundances near the coast of industrial regions, as confirmed by the observations presented here.

6 Discussion and conclusion

We find that there is a strong anthropogenic source of bromoform along the coast of East Asia with particular large contributions north of 20° N from the East China, Yellow and Japan Seas. This anthropogenic source results from local cooling water treatment in power plants and leads to extremely high annual mean air-sea flux rates of 3.1–9.1 nmol m^{-2} h^{-1} in coastal waters in East Asia. Atmospheric bromoform originating from industrial sources accumulates in the marine boundary layer and result in mixing ratios of up to 5–14 ppt. It shows a strong seasonal variability with the 'cloud of high bromoform abundances' being transported into the mid-latitudes during boreal summer and to the tropics during boreal winter.

In comparison, the bottom-up inventory by Ziska2013 shows much lower values along the coast of East Asia, but higher mean sea surface concentrations in Southeast Asia. Comparisons with individual campaigns suggest that our averaged anthropogenic values are higher than campaign-averaged estimates in surface water and air. This discrepancy of the mean values is possibly related to the regional extent of the campaign data, given the very sharp bromoform gradients from the coast into the open ocean waters. Maximum values found in surface water and air during the campaigns, however, agree very well with our estimates based on industrial sources for the LOW and MODERATE scenarios. Therefore, anthropogenic activities can be expected to cause extremely high bromoform concentrations and air-sea fluxes in locations relatively close to the source. Estimating the exact regional extent and distribution will require further targeted measurement campaigns.

Concentrations of bromoform in chemically treated cooling water from power plants depend on many different factors and observational studies provide a range of 8–290 µg L^{-1}. Based on the comparison of our model results to observations, we expect initial bromoform concentrations between 20–60 µg L^{-1} given by the two scenarios LOW and MODERATE. In consequence, oceanic and atmospheric abundances based on the HIGH scenario are most likely too high and only results based on the two lower scenarios are presented in this summary.

https://doi.org/10.5194/acp-2019-1004
Preprint. Discussion started: 27 January 2020

Our results indicate that cooling water from power plants provide a substantial and growing source of anthropogenic bromoform. Depending on the scenario, 100 to 300 Mmol bromine (Br) a^{-1} are released into the atmosphere from the coastal regions in Southeast and East Asia (LOW to MODERATE) in form of anthropogenic bromoform. The largest part, about 90 %, are emitted in coastal regions north of 20° N. In comparison, Ziska2013 estimates bromoform emissions of 34 Mmol Br a^{-1} for the same region north of 20° N. The high emissions of industrially produced bromoform in East Asia are most likely underrepresented in existing bottom-up estimates by Ziska et al. (2013) and Stemmler et al. (2015) and might explain some of their differences when compared to top-down estimates.

If bromoform is entrained into the stratosphere, it will contribute to ozone depletion driven by catalytic cycles. Atmospheric transport simulations show that during boreal winter strong northeasterly winds advect the anthropogenic bromoform from the East China Sea towards the tropics. Here it can be taken up by deep convection and reach the UTLS region. On average 0.19 ppt of bromoform are entrained above 17 km, the approximate altitude of the cold point, based on climatological and additional anthropogenic emissions. For the same configuration during boreal summer, the large amounts of anthropogenic bromoform emitted over the East China Sea do not reach the tropics, resulting in average mixing ratios of 0.17 ppt at 17 km. In comparison, the bottom-up Ziska2013 emissions are on average smaller, but spread out over a larger area thus resulting in similar total emissions, and only slightly less bromoform (0.15–0.16 ppt) is transported into the UTLS region during both seasons. In summary, the high anthropogenic bromoform emissions in the East China, Yellow and Japan Seas do not efficiently reach the stratosphere, unless the anthropogenic bromoform is advected with the Asian winter monsoon into the tropics, in which case it can lead to an increased entrainment of 14–19 % over this area.

Ashfold et al. (2015) and Oram et al. (2017) showed for chlorine-based VSLSs that pollution from East Asia can be efficiently entrained into the upper troposphere during DJF. Chlorine-based VSLSs concentrations of 50–250 ppt were measured at 10–12 km height (Oram et al., 2017). While chlorine-based species are still the largest contributor to ODSs, an increase in anthropogenic emission of brominated VSLSs is nevertheless of concern since bromine is about 60 times more effective in destroying ozone than chlorine (Sinnhuber et al., 2009). In particular during the northeasterly winter monsoon, many anthropogenic VSLSs from industrial emissions in East Asia can be entrained into the UTLS above the tropics.

While this study exclusively looks at the DBPs from cooling water treatment in power plants, other anthropogenic sources also contribute to local and global emissions of organic bromine, like desalination plants or ballast water from commercial ships which produce DBPs in chemically treated water. Desalination is mostly done at the Arabian Peninsula (Jones et al., 2019), and ballast water volumes with 3–5 billion m^3 a^{-1} (Tamelander et al., 2010) are globally negligible compared to cooling water volumes from coastal power plants but can locally increase DBP discharge (Maas et al., 2019). For assessing the total impact of anthropogenic VSLSs on a local industrial area, such as Singapore or the Pearl River Delta region, all sources of chemical water treatment need to be taken into account. Comparison of these two regions show that the bromoform from cooling water dominates

https://doi.org/10.5194/acp-2019-1004
Preprint. Discussion started: 27 January 2020

above ballast water, leading to emissions of around 990 pmol m^{-2} h^{-1} in Singapore and 6430 pmol m^{-2} h^{-1} in the Pearl River Delta (MODERATE, Figure 5b), while bromoform from ballast water is expected to cause 900 and 2000 pmol m^{-2} h^{-1} for these two areas (Maas et al., 2019). Direct outgassing during treatment of circulating water through the cooling towers into the atmosphere can also occur which has not been quantified yet and is therefore not considered here. Overall, cooling water from power plants can be assumed to be the largest global source of anthropogenic bromoform as it has by far the largest water volumes and is present in all regions and climate zones. The contribution of bromoform from anthropogenic sources should be considered as relevant next to natural sources for future estimates of the atmospheric bromine input.

Acknowledgements

The OGCM model data used for this study were kindly provided through collaboration within the DRAKKAR framework by the National Oceanographic Centre, Southampton, UK. We especially thank Andrew C. Coward, Adrian L. New and colleagues for making the data available. The OGCM and trajectory simulations were performed in the High-Performance Computing Centre at the Christian-Albrechts-Universität zu Kiel. Furthermore, we wish to thank Bruno Blanke and Nicolas Grima for realising and providing the Lagrangian software ARIANE; and Siren Rühs for helping with the set-up of the ARIANE environment. This study was carried out within the Emmy-Noether group AVeSH (A new threat to the stratospheric ozone layer from Anthropogenic Very Short-lived Halocarbons) funded by the Deutsche Forschungsgemeinschaft (DFG, German Research Foundation) – TE 1134/1. JVD acknowledges the Helmholtz-Gemeinschaft and the GEOMAR Helmholtz Centre for Ocean Research Kiel (grant IV014/GH018).

Author contribution

JM wrote the manuscript, performed the Lagrangian ocean simulations and created the output. YJ performed the Lagrangian simulations in the atmosphere. ST developed the research question and guided the research process. BQ developed the research question and gave input on the observational data. AB and JVD provided the NEMO-ORCA model data and gave input on the ocean simulations. All authors took part in the process of the manuscript preparation.

The authors declare that they have no conflict of interest.

Data availability

Data from the ARIANE and FLEXPART simulations are available upon request from the corresponding author.

https://doi.org/10.5194/acp-2019-1004
Preprint. Discussion started: 27 January 2020

Atmospheric Chemistry and Physics Discussions

References

Allonier, A.-S., Khalanski, M., Camel, V. and Bermond, A.: Characterization of Chlorination By-products in Cooling Effluents of Coastal Nuclear Power Stations, Mar. Pollut. Bull., 38(12), 1232–1241, doi:10.1016/S0025-326X(99)00168-X, 1999.

Aschmann, J. and Sinnhuber, B.-M.: Contribution of very short-lived substances to stratospheric bromine loading: uncertainties and constraints, Atmos. Chem. Phys., 13(3), 1203–1219, doi:10.5194/acp-13-1203-2013, 2013.

Aschmann, J., Sinnhuber, B.-M., Atlas, E. L. and Schauffler, S. M.: Modeling the transport of very short-lived substances into the tropical upper troposphere and lower stratosphere, Atmos. Chem. Phys., 9(23), 9237–9247, doi:10.5194/acp-9-9237-2009, 2009.

Ashfold, M. J., Pyle, J. A., Robinson, A. D., Meneguz, E., Nadzir, M. S. M., Phang, S. M., Samah, A. A., Ung, H. E., Peng, L. K., Yong, S. E. and Harris, N. R. P.: Rapid transport of East Asian pollution to the deep tropics, Atmos. Chem. Phys., 15, 3565–3573, doi:10.5194/acp-15-3565-2015, 2015.

Blanke, B., Arhan, M., Madec, G. and Roche, S.: Warm Water Paths in the Equatorial Atlantic as Diagnosed with a General Circulation Model, J. Phys. Oceanogr., 29(11), 2753–2768, doi:10.1175/1520-0485(1999)029<2753:WWPITE>2.0.CO;2, 1999.

Boudjellaba, D., Dron, J., Revenko, G., Démelas, C. and Boudenne, J.-L.: Chlorination by-product concentration levels in seawater and fish of an industrialised bay (Gulf of Fos, France) exposed to multiple chlorinated effluents, Sci. Total Environ., 541, 391–399, doi:10.1016/j.scitotenv.2015.09.046, 2016.

Dee, D. P., Uppala, S. M., Simmons, A. J., Berrisford, P., Poli, P., Kobayashi, S., Andrae, U., Balmaseda, M. A., Balsamo, G., Bauer, P., Bechtold, P., Beljaars, A. C. M., van de Berg, L., Bidlot, J., Bormann, N., Delsol, C., Dragani, R., Fuentes, M., Geer, A. J., Haimberger, L., Healy, S. B., Hersbach, H., Hólm, E. V., Isaksen, L., Kållberg, P., Köhler, M., Matricardi, M., McNally, A. P., Monge-Sanz, B. M., Morcrette, J.-J., Park, B.-K., Peubey, C., de Rosnay, P., Tavolato, C., Thépaut, J.-N. and Vitart, F.: The ERA-Interim reanalysis: configuration and performance of the data assimilation system, Q. J. R. Meteorol. Soc., 137(656), 553–597, doi:10.1002/qj.828, 2011.

Dussin, R., Barnier, B., Brodeau, L. and Molines, J. M.: The Making Of the DRAKKAR FORCING SET DFS5, DRAKKAR/MyOcean Rep. 01-04-16, 2016(April), 1–34, 2016.

Engel, A., Rigby, M. (Lead A., Burkholder, J. B., Fernandez, R. P., Froidevaux, L., Hall, B. D., Hossaini, R., Saito, T., Vollmer, M. K. and Yao, B.: Update on Ozone-Depleting Substances (ODSs) and Other Gases of Interest to the Montreal Protocol, Chapter 1, in Scientific Assessment of Ozone Depletion: 2018, Global Ozone Research and Monitoring Project – Report No. 58., 2018.

Fiehn, A., Quack, B., Hepach, H., Fuhlbrügge, S., Tegtmeier, S., Toohey, M., Atlas, E. and Krüger, K.: Delivery of halogenated very short-lived substances from the west Indian Ocean to the stratosphere during the Asian summer monsoon, Atmos. Chem. Phys., 17(11), 6723–6741, doi:10.5194/acp-17-6723-2017, 2017.

Fiehn, A., Quack, B., Stemmler, I., Ziska, F. and Krüger, K.: Importance of seasonally resolved oceanic emissions for bromoform delivery from the tropical Indian Ocean and west Pacific to the stratosphere, Atmos. Chem. Phys., 18(16), 11973–11990, doi:10.5194/acp-18-11973-2018, 2018.

Fogelqvist, E. and Krysell, M.: Naturally and anthropogenically produced bromoform in the Kattegatt, a semi-enclosed oceanic basin, J. Atmos. Chem., 13(4), 315–324, doi:10.1007/BF00057749, 1991.

Fuhlbrügge, S., Quack, B., Tegtmeier, S., Atlas, E., Hepach, H., Shi, Q., Raimund, S. and Krüger, K.: The contribution of oceanic halocarbons to marine and free tropospheric air over the tropical West Pacific, Atmos. Chem. Phys., 16(12), 7569–7585, doi:10.5194/acp-16-7569-2016, 2016.

He, Z., Yang, G.-P., Lu, X.-L. and Zhang, H.-H.: Distributions and sea-to-air fluxes of chloroform, trichloroethylene, tetrachloroethylene, chlorodibromomethane and bromoform in the Yellow Sea and the East China Sea during spring, Environ. Pollut., 177, 28–37, doi:10.1016/j.envpol.2013.02.008, 2013a.

https://doi.org/10.5194/acp-2019-1004
Preprint. Discussion started: 27 January 2020

He, Z., Yang, G.-P. and Lu, X.-L.: Distributions and sea-to-air fluxes of volatile halocarbons in the East China Sea in early winter, Chemosphere, 90(2), 747–757, doi:10.1016/j.chemosphere.2012.09.067, 2013b.

Helz, G. R., Sugam, R. and Sigleo, A. C.: Chemical modifications of estuarine water by a power plant using continuous chlorination, Environ. Sci. Technol., 18(3), 192–199, doi:10.1021/es00121a011, 1984.

Hossaini, R., Mantle, H., Chipperfield, M. P., Montzka, S. A., Hamer, P., Ziska, F., Quack, B., Krüger, K., Tegtmeier, S., Atlas, E., Sala, S., Engel, A., Bönisch, H., Keber, T., Oram, D., Mills, G., Ordóñez, C., Saiz-Lopez, A., Warwick, N., Liang, Q., Feng, W., Moore, F., Miller, B. R., Marécal, V., Richards, N. A. D., Dorf, M. and Pfeilsticker, K.: Evaluating global emission inventories of biogenic bromocarbons, Atmos. Chem. Phys., 13(23), 11819–11838, doi:10.5194/acp-13-11819-2013, 2013.

Hossaini, R., Chipperfield, M. P., Montzka, S. A., Rap, A., Dhomse, S. and Feng, W.: Efficiency of short-lived halogens at influencing climate through depletion of stratospheric ozone, Nat. Geosci., 8(3), 186–190, doi:10.1038/ngeo2363, 2015.

Hossaini, R., Patra, P. K., Leeson, A. A., Krysztofiak, G., Abraham, N. L., Andrews, S. J., Archibald, A. T., Aschmann, J., Atlas, E. L., Belikov, D. A., Bönisch, H., Carpenter, L. J., Dhomse, S., Dorf, M., Engel, A., Feng, W., Fuhlbrügge, S., Griffiths, P. T., Harris, N. R. P., Hommel, R., Keber, T., Krüger, K., Lennartz, S. T., Maksyutov, S., Mantle, H., Mills, G. P., Miller, B., Montzka, S. A., Moore, F., Navarro, M. A., Oram, D. E., Pfeilsticker, K., Pyle, J. A., Quack, B., Robinson, A. D., Saikawa, E., Saiz-Lopez, A., Sala, S., Sinnhuber, B. M., Taguchi, S., Tegtmeier, S., Lidster, R. T., Wilson, C. and Ziska, F.: A multi-model intercomparison of halogenated very short-lived substances (TransCom-VSLS): Linking oceanic emissions and tropospheric transport for a reconciled estimate of the stratospheric source gas injection of bromine, Atmos. Chem. Phys., 16(14), 9163–9187, doi:10.5194/acp-16-9163-2016, 2016.

IEA: Key world energy statistics 2005, Int. Energy Agency, 2005.

IEA: Key world energy statistics 2018, Int. Energy Agency, 2018.

Jenner, H. A., Taylor, C. J. L., van Donk, M. and Khalanski, M.: Chlorination by-products in chlorinated cooling water of some European coastal power stations, Mar. Environ. Res., 43(4), 279–293, doi:10.1016/S0141-1136(96)00091-8, 1997.

Jia, Y., Tegtmeier, S., Atlas, E. and Quack, B.: How marine emissions of bromoform impact the remote atmosphere, Atmos. Chem. Phys., 19(17), 11089–11103, doi:10.5194/acp-19-11089-2019, 2019.

Joint Research Council: Integrated Pollution Prevention and Control (IPPC) Reference Document on the application of Best Available Techniques to Industrial Cooling Systems, Eur. Comm., (December), 335, 2001.

Jones, E., Qadir, M., Vliet, M. T. H. Van, Smakhtin, V. and Kang, S.: Science of the Total Environment The state of desalination and brine production : A global outlook, Sci. Total Environ., 657, 1343–1356, doi:10.1016/j.scitotenv.2018.12.076., 2019.

Liu, Z., Wang, X., Luo, Z., Huo, M., Wu, J., Huo, H. and Yang, W.: Removing of Disinfection By-Product Precursors from Surface Water by Using Magnetic Graphene Oxide, edited by Y. K. Mishra, PLoS One, 10(12), e0143819, doi:10.1371/journal.pone.0143819, 2015.

Maas, J., Tegtmeier, S., Quack, B., Biastoch, A., Durgadoo, J. V., Rühs, S., Gollasch, S. and David, M.: Simulating the spread of disinfection by-products and anthropogenic bromoform emissions from ballast water discharge in Southeast Asia, Ocean Sci., 15(4), 891–904, doi:10.5194/os-15-891-2019, 2019.

Madec, G. and the N. T.: NEMO ocean engine, Note du Pôle modélisation l'Institut Pierre-Simon Laplace No 27, (27), 2008.

Moat, B. I., Josey, S. A., Sinha, B., Blaker, A. T., Smeed, D. A., McCarthy, G. D., Johns, W. E., Hirschi, J. J. M., Frajka-Williams, E., Rayner, D., Duchez, A. and Coward, A. C.: Major variations in subtropical North Atlantic heat transport at short (5 day) timescales and their causes, J. Geophys. Res. Ocean., doi:10.1002/2016JC011660, 2016.

Montzka, S. a. and Reimann, S.: Ozone-Depleting Substances (ODSs) and Related Chemicals, Sci. Assess. Ozone Deplet. 2010, Chapter 1, 1–108, 2010.

Montzka, S. A., Dutton, G. S., Yu, P., Ray, E., Portmann, R. W., Daniel, J. S., Kuijpers, L., Hall, B. D., Mondeel, D., Siso, C., Nance, J. D., Rigby, M., Manning, A. J., Hu, L., Moore, F., Miller, B. R. and Elkins, J. W.: An unexpected and persistent increase in global emissions of ozone-depleting CFC-11, Nature, doi:10.1038/s41586-018-0106-2, 2018.

Nadzir, M. S. M., Phang, S. M., Abas, M. R., Abdul Rahman, N., Abu Samah, A., Sturges, W. T., Oram, D. E., Mills, G. P., Leedham, E. C., Pyle, J. A., Harris, N. R. P., Robinson, A. D., Ashfold, M. J., Mead, M. I., Latif, M. T., Khan, M. F., Amiruddin, A. M., Banan, N. and Hanafiah, M. M.: Bromocarbons in the tropical coastal and open ocean atmosphere during the 2009 Prime Expedition Scientific Cruise (PESC-09), Atmos. Chem. Phys., 14(15), 8137–8148, doi:10.5194/acp-14-8137-2014, 2014.

Nightingale, D., Malin, G., Law, C. S., Watson, A. J., Liss, P. S., Liddicoat, M. I., Boutin, J. and Upstill-Goddard, R. C.: In situ evaluation of air-sea gas exchange parameterizations using novel conservative and volatile tracers, Global Biogeochem. Cycles, 14(1), 373–387, 2000.

Oram, D. E., Ashfold, M. J., Laube, J. C., Gooch, L. J., Humphrey, S., Sturges, W. T., Leedham-Elvidge, E., Forster, G. L., Harris, N. R. P., Iqbal Mead, M., Samah, A. A., Phang, S. M., Ou-Yang, C. F., Lin, N. H., Wang, J. L., Baker, A. K., Brenninkmeijer, C. A. M. and Sherry, D.: A growing threat to the ozone layer from short-lived anthropogenic chlorocarbons, Atmos. Chem. Phys., 17(19), 11929–11941, doi:10.5194/acp-17-11929-2017, 2017.

Padhi, R. K., Subramanian, S., Mohanty, A. K., Bramha, S. N., Prasad, M. V. R. R. and Satpathy, K. K.: Trihalomethanes in the Cooling Discharge of a Power Plant on Chlorination of Intake Seawater, Environ. Eng. Res., 17(S1), 57–62, doi:10.4491/eer.2012.17.S1.S57, 2012.

Quack, B. and Wallace, D. W. R.: Air-sea flux of bromoform: Controls, rates, and implications, Global Biogeochem. Cycles, 17(1), 1023, doi:10.1029/2002GB001890, 2003.

Rajamohan, R., Vinnitha, E., Venugopalan, V. P. and Narasimhan, S. V: Chlorination by-products and their discharge from the cooling water system of a coastal electric plant, Curr. Sci., 93(11), 1608–1612, 2007.

Rigby, M., Park, S., Saito, T., Western, L. M., Redington, A. L., Fang, X., Henne, S., Manning, A. J., Prinn, R. G., Dutton, G. S., Fraser, P. J., Ganesan, A. L., Hall, B. D., Harth, C. M., Kim, J., Kim, K.-R., Krummel, P. B., Lee, T., Li, S., Liang, Q., Lunt, M. F., Montzka, S. A., Mühle, J., O'Doherty, S., Park, M.-K., Reimann, S., Salameh, P. K., Simmonds, P., Tunnicliffe, R. L., Weiss, R. F., Yokouchi, Y. and Young, D.: Increase in CFC-11 emissions from eastern China based on atmospheric observations, Nature, 569(7757), 546–550, doi:10.1038/s41586-019-1193-4, 2019.

Saiz-Lopez, A. and von Glasow, R.: Reactive halogen chemistry in the troposphere, Chem. Soc. Rev., 41(19), 6448, doi:10.1039/c2cs35208g, 2012.

Sherry, D., McCulloch, A., Liang, Q., Reimann, S. and Newman, P. A.: Current sources of carbon tetrachloride (CCl 4) in our atmosphere, Environ. Res. Lett., 13(2), 024004, doi:10.1088/1748-9326/aa9c87, 2018.

Sherwen, T., Schmidt, J. A., Evans, M. J., Carpenter, L. J., Großmann, K., Eastham, S. D., Jacob, D. J., Dix, B., Koenig, T. K., Sinreich, R., Ortega, I., Volkamer, R., Saiz-Lopez, A., Prados-Roman, C., Mahajan, A. S. and Ordóñez, C.: Global impacts of tropospheric halogens (Cl, Br, I) on oxidants and composition in GEOS-Chem, Atmos. Chem. Phys., 16(18), 12239–12271, doi:10.5194/acp-16-12239-2016, 2016.

Sinnhuber, B.-M., Sheode, N., Sinnhuber, M., Chipperfield, M. P. and Feng, W.: The contribution of anthropogenic bromine emissions to past stratospheric ozone trends: a modelling study, Atmos. Chem. Phys., 9(8), 2863–2871, doi:10.5194/acp-9-2863-2009, 2009.

Stemmler, I., Hense, I. and Quack, B.: Marine sources of bromoform in the global open ocean – global patterns and emissions, Biogeosciences, 12(6), 1967–1981, doi:10.5194/bg-12-1967-2015, 2015.

Stohl, A., Forster, C., Frank, A., Seibert, P. and Wotawa, G.: Technical note: The Lagrangian particle dispersion model FLEXPART version 6.2, Atmos. Chem. Phys., 5(9), 2461–2474, doi:10.5194/acp-5-2461-2005, 2005.

https://doi.org/10.5194/acp-2019-1004
Preprint. Discussion started: 27 January 2020

Tamelander, J., Riddering, L., Haag, F. and Matheickal, J.: Guidelines for development of a national ballast water management strategy, GEF-UNDP-IMO Glob. London, UK IUCN, Gland. Switz., GloBallast(No. 18) [online] Available from: http://globallast.imo.org/wp-content/uploads/2014/11/Mono18_English.pdf, 2010.

Taylor, C. J. L.: The effects of biological fouling control at coastal and estuarine power stations, Mar. Pollut. Bull., 53(1–4), 30–48, doi:10.1016/j.marpolbul.2006.01.004, 2006.

Tegtmeier, S., Ziska, F., Pisso, I., Quack, B., Velders, G. J. M., Yang, X. and Krüger, K.: Oceanic bromoform emissions weighted by their ozone depletion potential, Atmos. Chem. Phys., 15(23), 13647–13663, doi:10.5194/acp-15-13647-2015, 2015.

Tegtmeier, S., Atlas, E., Quack, B., Ziska, F. and Krüger, K.: Variability and long-term changes of brominated VSLS at the tropical tropopause, Atmos. Chem. Phys. Discuss., 1–44, doi:10.5194/acp-2019-490, 2019.

Waliser, D. E. and Gautier, C.: A satellite-derived climatology of the ITCZ, J. Clim., 6(11), 2162–2174, doi:10.1175/1520-0442(1993)006<2162:ASDCOT>2.0.CO;2, 1993.

Yang, B., Yang, G.-P., Lu, X.-L., Li, L. and He, Z.: Distributions and sources of volatile chlorocarbons and bromocarbons in the Yellow Sea and East China Sea, Mar. Pollut. Bull., 95(1), 491–502, doi:10.1016/j.marpolbul.2015.03.009, 2015.

Yang, G.-P., Yang, B., Lu, X.-L., Ding, H.-B. and He, Z.: Spatio-temporal variations of sea surface halocarbon concentrations and fluxes from southern Yellow Sea, Biogeochemistry, 121(2), 369–388, doi:10.1007/s10533-014-0007-x, 2014.

Yang, J. S.: Bromoform in the effluents of a nuclear power plant: A potential tracer of coastal water masses, Hydrobiologia, 464, 99–105, doi:10.1023/A:1013922731434, 2001.

Yokouchi, Y., Saito, T., Zeng, J., Mukai, H. and Montzka, S.: Seasonal variation of bromocarbons at Hateruma Island, Japan: implications for global sources, J. Atmos. Chem., 74(2), 171–185, doi:10.1007/s10874-016-9333-9, 2017.

Ziska, F., Quack, B., Abrahamsson, K., Archer, S. D., Atlas, E., Bell, T., Butler, J. H., Carpenter, L. J., Jones, C. E., Harris, N. R. P. P., Hepach, H., Heumann, K. G., Hughes, C., Kuss, J., Krüger, K., Liss, P., Moore, R. M., Orlikowska, A., Raimund, S., Reeves, C. E., Reifenhäuser, W., Robinson, A. D., Schall, C., Tanhua, T., Tegtmeier, S., Turner, S., Wang, L., Wallace, D., Williams, J., Yamamoto, H., Yvon-Lewis, S. and Yokouchi, Y.: Global sea-to-air flux climatology for bromoform, dibromomethane and methyl iodide, Atmos. Chem. Phys., 13(17), 8915–8934, doi:10.5194/acp-13-8915-2013, 2013.

https://doi.org/10.5194/acp-2019-1004
Preprint. Discussion started: 27 January 2020

Atmospheric Chemistry and Physics Discussions

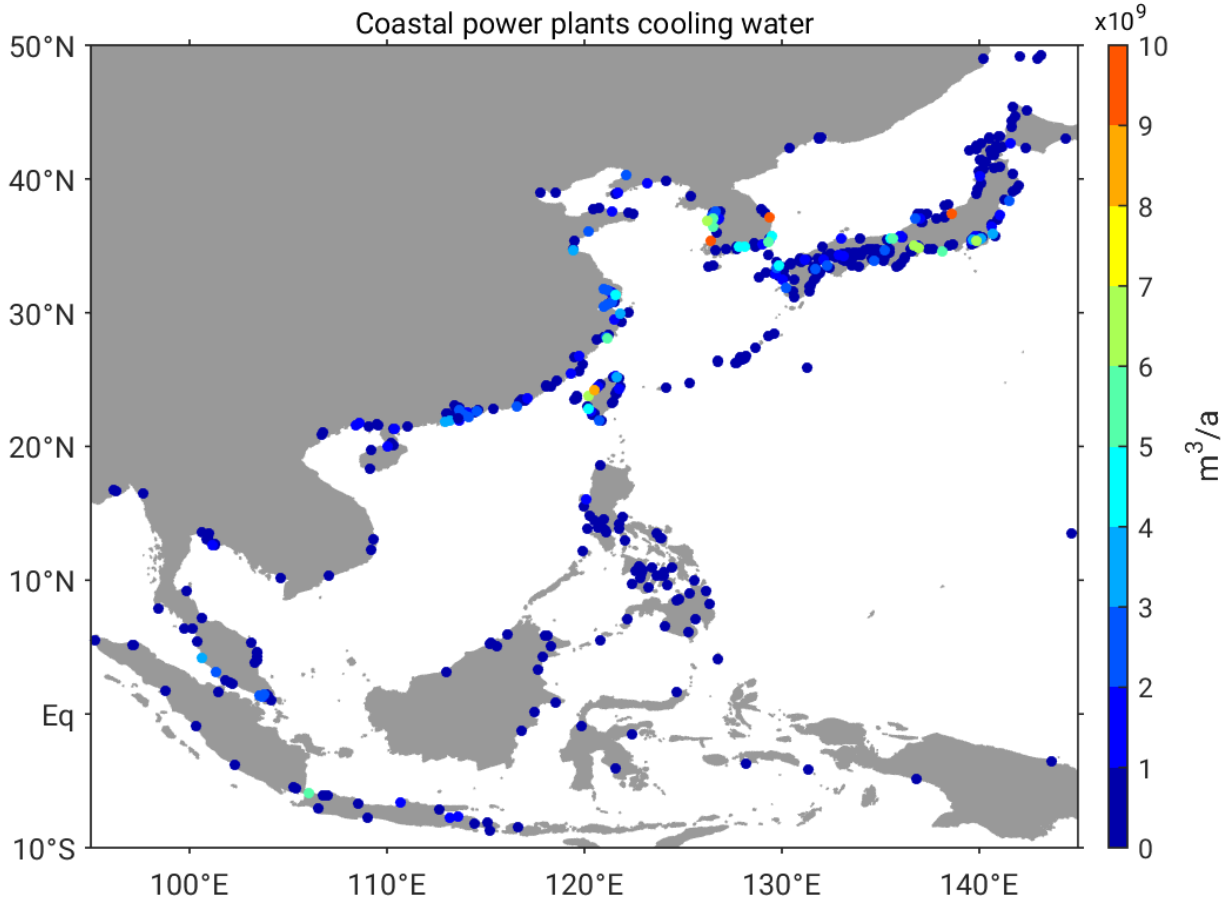

Figure 1: Location and annual cooling water volume [billion m^3 a^{-1}] of coastal power plants in East and Southeast Asia extracted from the enipedia-database and color-coded by the cooling water discharge.

https://doi.org/10.5194/acp-2019-1004
Preprint. Discussion started: 27 January 2020

Atmospheric Chemistry and Physics Discussions

Table 1: Bromoform concentrations measured in water samples from power plant cooling water and surrounding waters. Measurements in the power plant effluent can refer to both, samples of the undiluted water stream or sea water samples at the outlet.

Power plant effluent/ near outlet		Surroundings		Location	Reference
µg L^{-1}	nmol L^{-1}	µg L^{-1}	nmol L^{-1}		
90-100	356-396	1-20	4-79	Gothenburg, Sweden, Kattegatt	Fogelqvist, 1991
9-17	35-67	0.1-5	0.4-20	North Sea	Jenner, 1997
8-27	32-107	n/a	n/a	English Channel	Allonier, 1999
124	495	1-50	4-200	Youngkwang, South Korea, Yellow Sea	Yang, 2001
20-290	79-1147	0-54	0-214	Kalpakkam, India, Bay of Bengal	Rajamohan, 2007
12-41	47-162	n/a	n/a	Kalpakkam, India, Bay of Bengal	Padhi, 2012
19	75	0.5-2.2	2-9	Gulf of Fos, France, Mediterranean	Boudjellaba, 2016

https://doi.org/10.5194/acp-2019-1004
Preprint. Discussion started: 27 January 2020

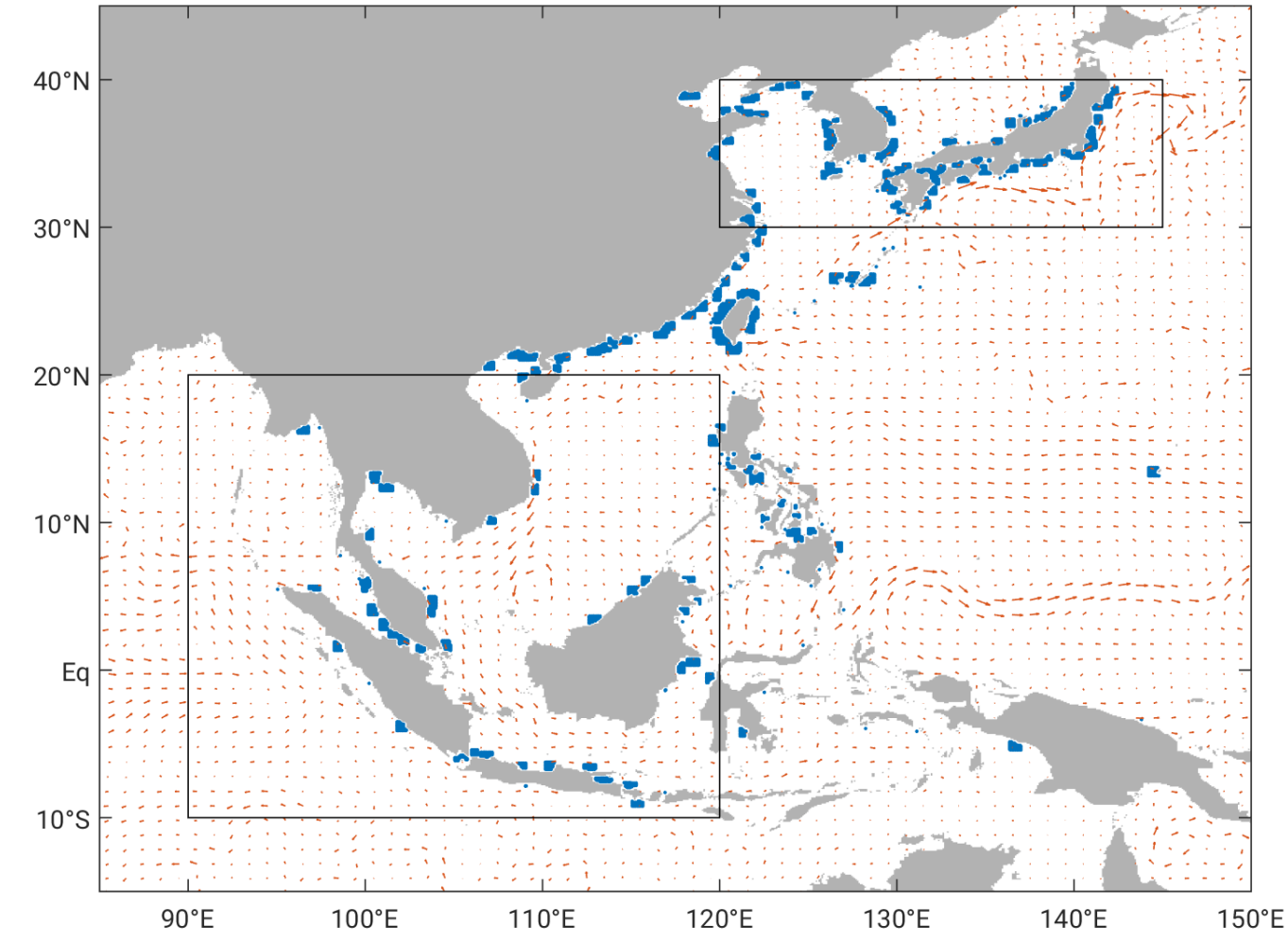

Figure 2: Initial position of particles in East and Southeast Asia (blue dots). NEMO-ORCA12 ocean currents from the initialisation time in January 2005 (red arrows); and the two boxes which mark the region referred to as tropics and subtropics as described in section 2.3.

https://doi.org/10.5194/acp-2019-1004
Preprint. Discussion started: 27 January 2020

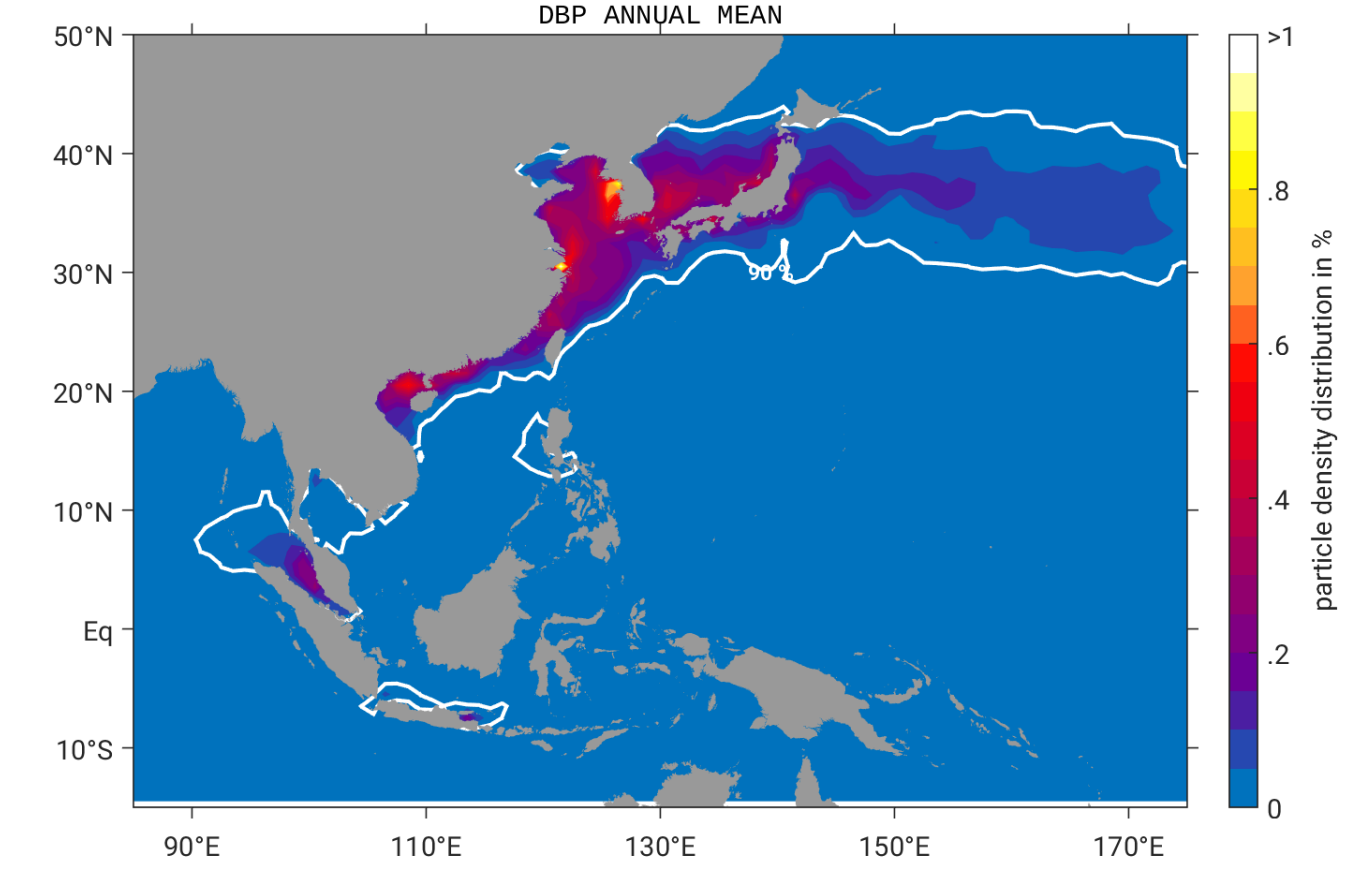

Figure 3: Annual mean particle density distribution in % of DBPs from cooling water treatment in coastal power plants in East and Southeast Asia. The white contour line shows the patches where 90 % of the largest particle density are located.

https://doi.org/10.5194/acp-2019-1004
Preprint. Discussion started: 27 January 2020

Atmospheric Chemistry and Physics Discussions

Table 2: Average values for the three scenarios LOW, MODERATE, HIGH, as well as the climatological values from the Ziska2013 bottom-up estimate in East and Southeast Asia. Sea surface concentrations [pmol L^{-1}], air-sea flux [pmol m^{-2} h^{-1}] and atmospheric mixing ratios from Ziska-EastAsia in the marine boundary layer [ppt] are given as the mean and the standard deviation over the largest 90 % (referred to as mean values) and over the largest 10 % (referred to as maximum values). The annual mean bromine flux [Mmol Br a^{-1}] is derived from the air-sea flux of the total domain in East and Southeast Asia.

Scenario	Sea surface concentration		Air-sea flux		Br flux	Atmospheric mixing ratio JJA		DJF	
	Mean	Max	Mean	Max	Total	Mean	Max	Mean	Max
LOW	23±24	112.1±6.3	3.1±3.4	13.7±0.9	100	0.5±0.6	4.6±1.2	0.3±0.4	3.2±1.5
MODERATE	68±74	338.3±16.6	9.1±10.2	41.1±2.9	300	1.6±2.0	13.9±3.4	0.9±1.3	9.5±4.6
HIGH	113±122	563.6±28.8	15.1±16.9	68.5±4.7	500	2.4±3.3	23.3±5.5	1.5±2.2	15.9±8.3
Ziska-EastAsia	7±6	21.3±1.3	0.4±0.2	1.1±0.2	118	0.2±0.2	0.8±0.1	0.2±0.1	0.5±0.1

https://doi.org/10.5194/acp-2019-1004
Preprint. Discussion started: 27 January 2020

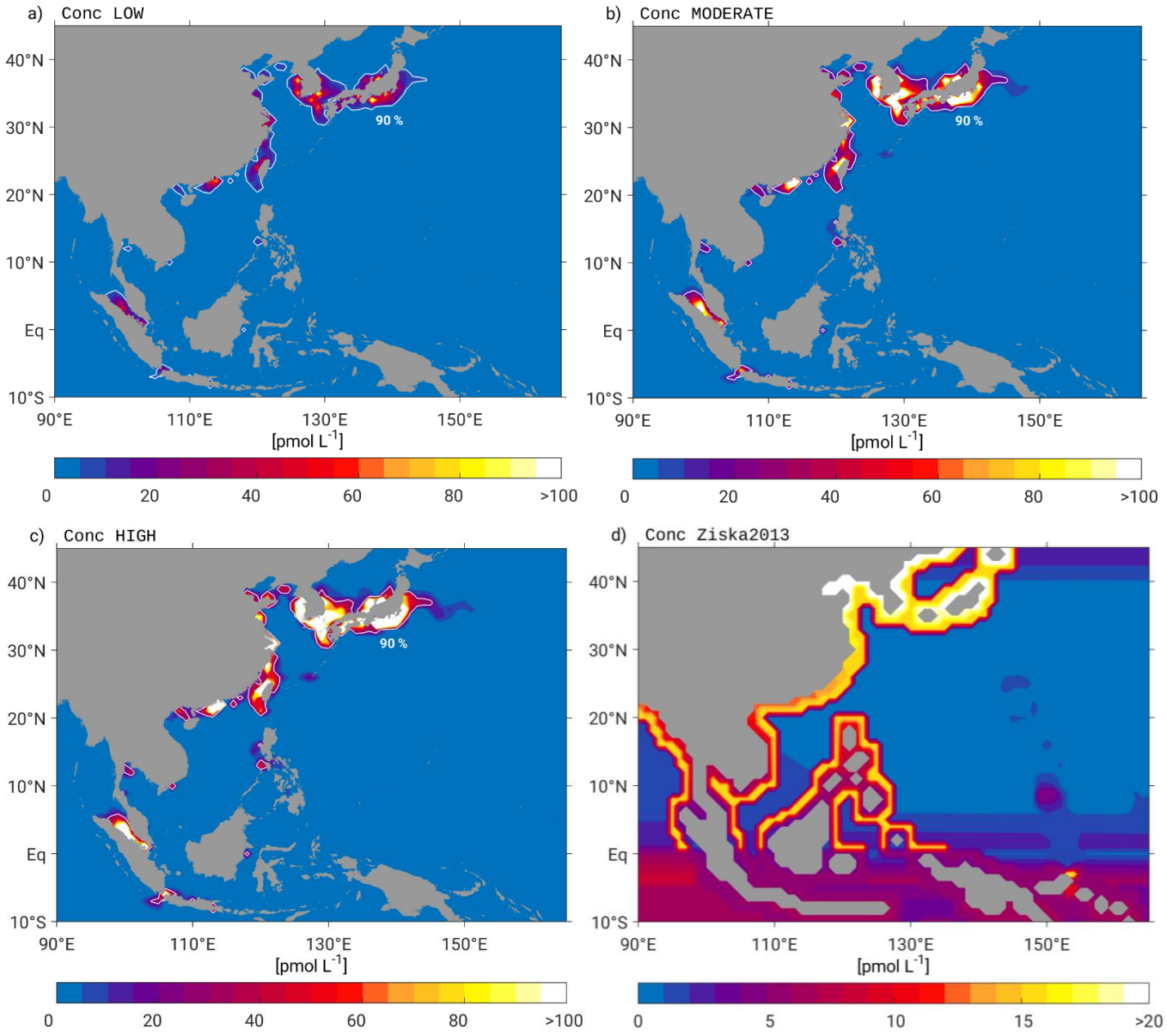

Figure 4: Annual mean surface bromoform concentration in pmol L^{-1} for the three scenarios a) LOW, b) MODERATE and c) HIGH as well as d) the bromoform surface map updated from Ziska2013. Note, that the colorbar for d) varies from the limits in a)-c). The white contour line in panel a)-c) shows the patches where 90 % of the largest concentrations are located.

https://doi.org/10.5194/acp-2019-1004
Preprint. Discussion started: 27 January 2020

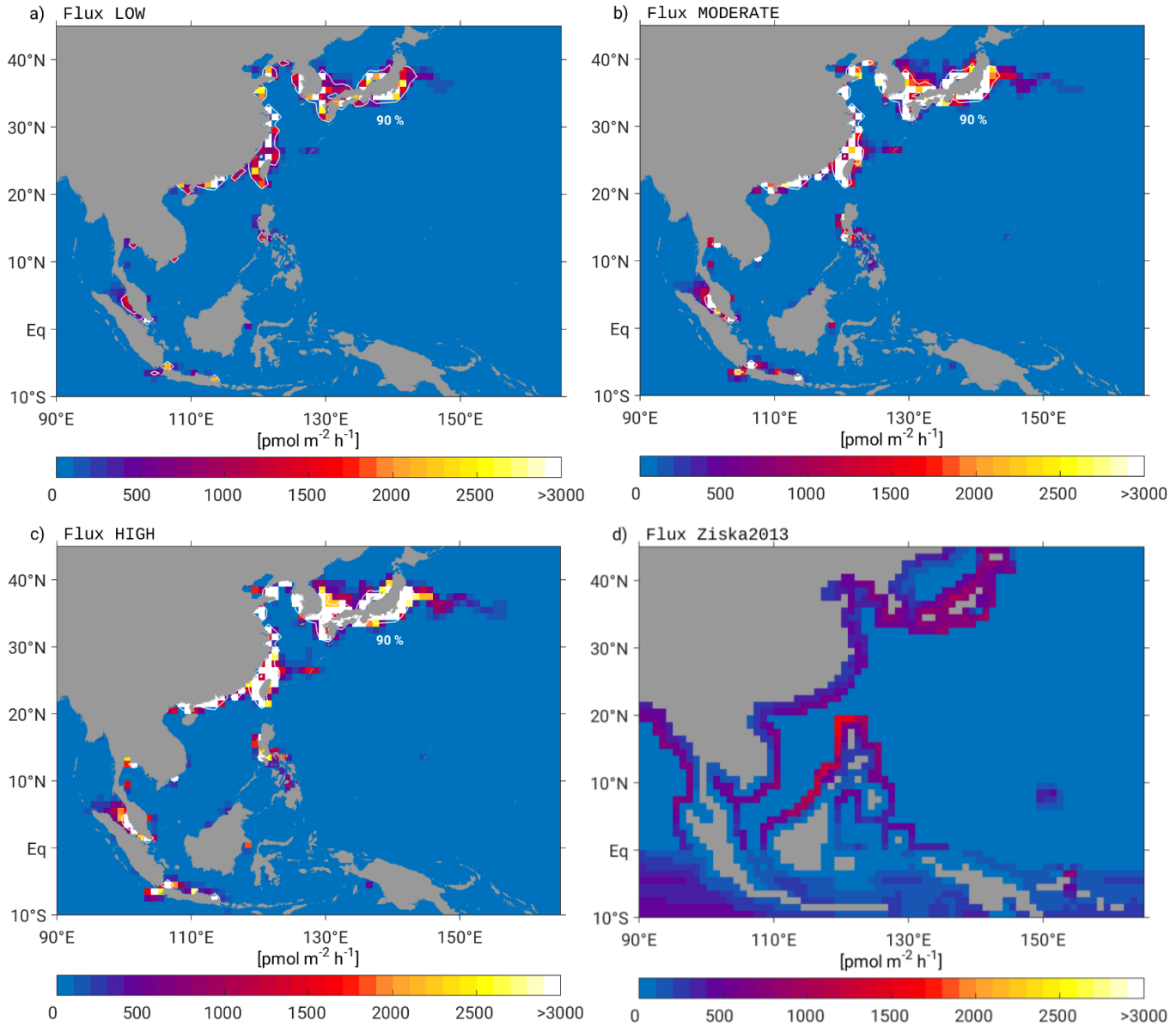

Figure 5: Annual mean air-sea flux of bromoform in pmol m^{-2} h^{-1} for the three scenarios a) LOW, b) MODERATE, c) HIGH, as well as d) the air-sea flux calculated from updated ocean and atmospheric maps after Ziska2013. The white contour line in panel a)-c) shows the patches where 90 % of the largest emissions are located.

https://doi.org/10.5194/acp-2019-1004
Preprint. Discussion started: 27 January 2020

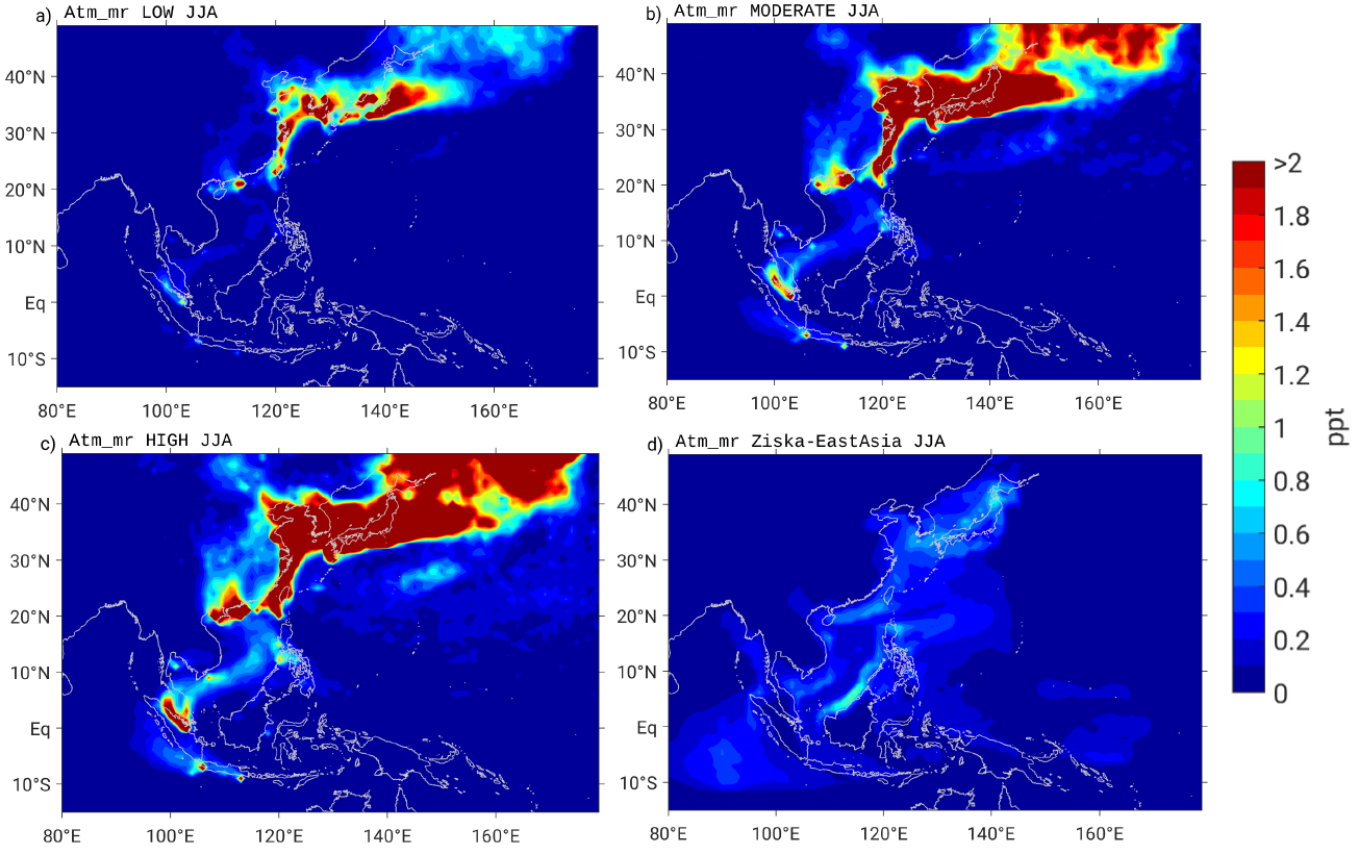

Figure 6: 5-day mean bromoform mixing ratios [ppt] in 50 m height during JJA derived from FLEXPART runs driven by the three scenarios a) LOW, b) MODERATE, c) HIGH, and d) Ziska2013-EastAsia.

https://doi.org/10.5194/acp-2019-1004
Preprint. Discussion started: 27 January 2020

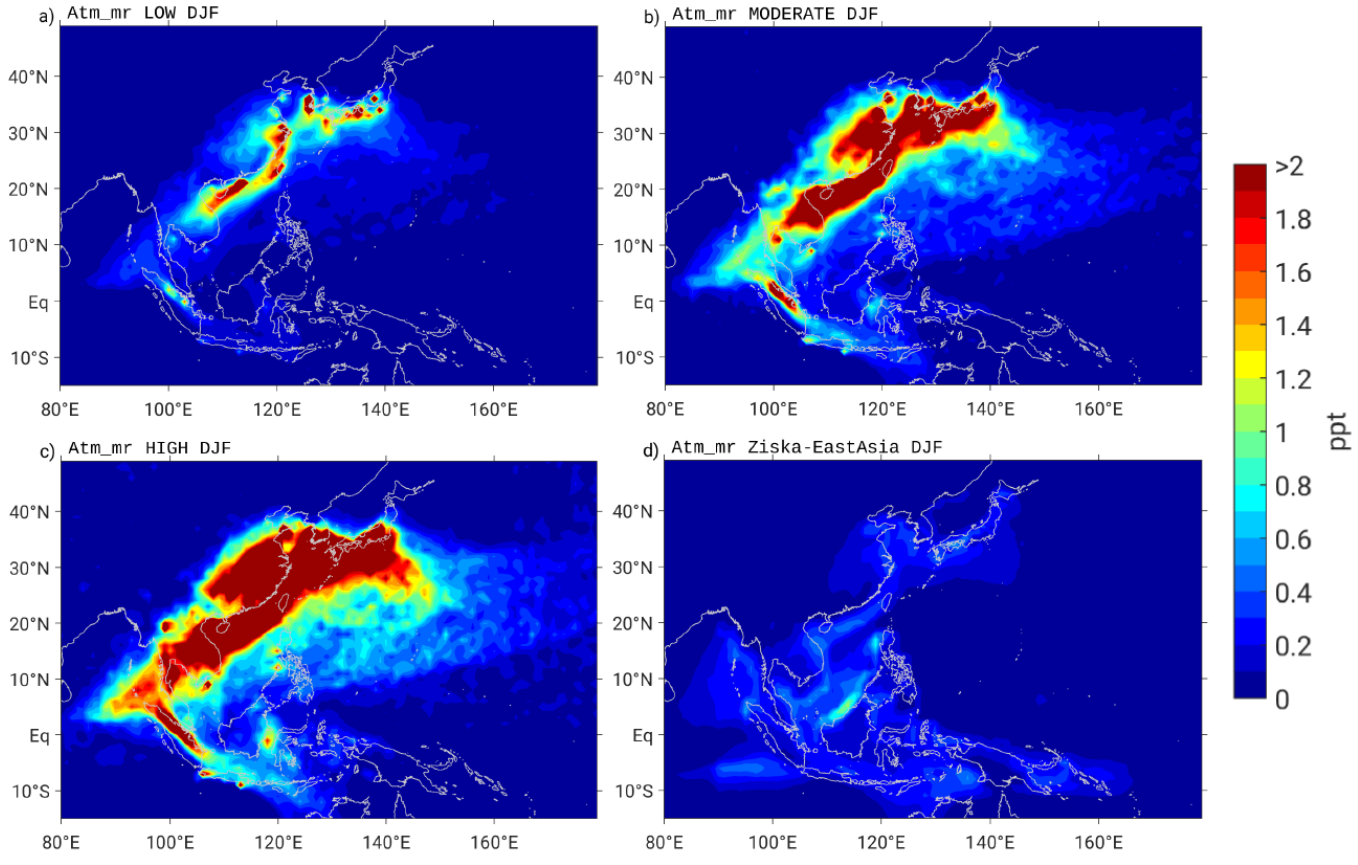

Figure 7: Same as Figure 6 only during DJF.

https://doi.org/10.5194/acp-2019-1004
Preprint. Discussion started: 27 January 2020

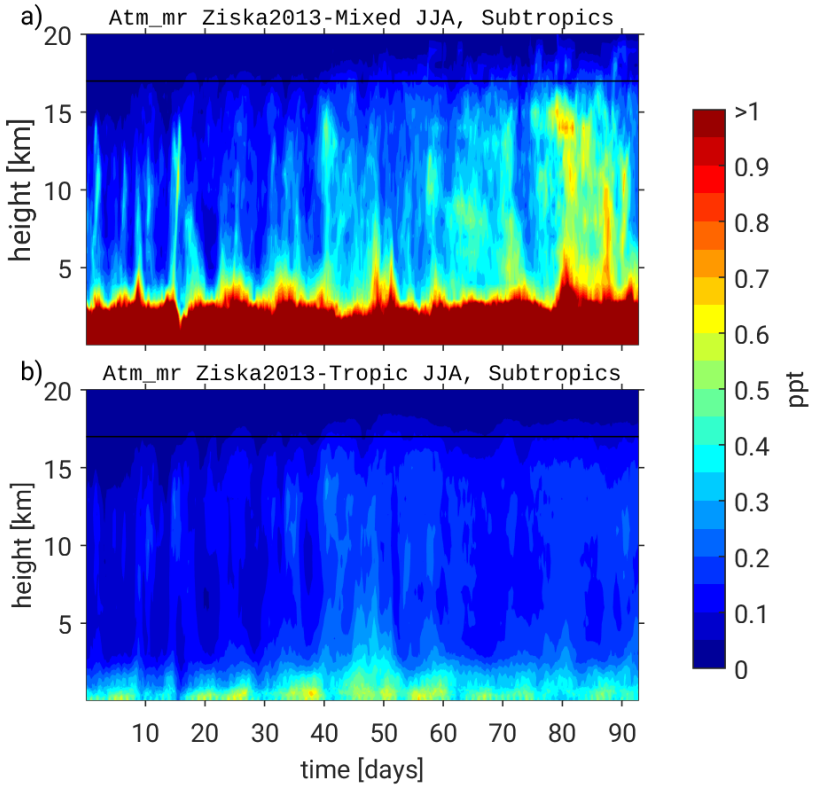

Figure 8: Time series of bromoform mixing ratio [ppt] in the subtropics (30° N–40° N, 120° E–145° E) during JJA for a) the Ziska2013-Mixed run and b) the Ziska2013-Tropics run. The black line marks the approximate location of the cold point tropopause at 17 km.

https://doi.org/10.5194/acp-2019-1004
Preprint. Discussion started: 27 January 2020

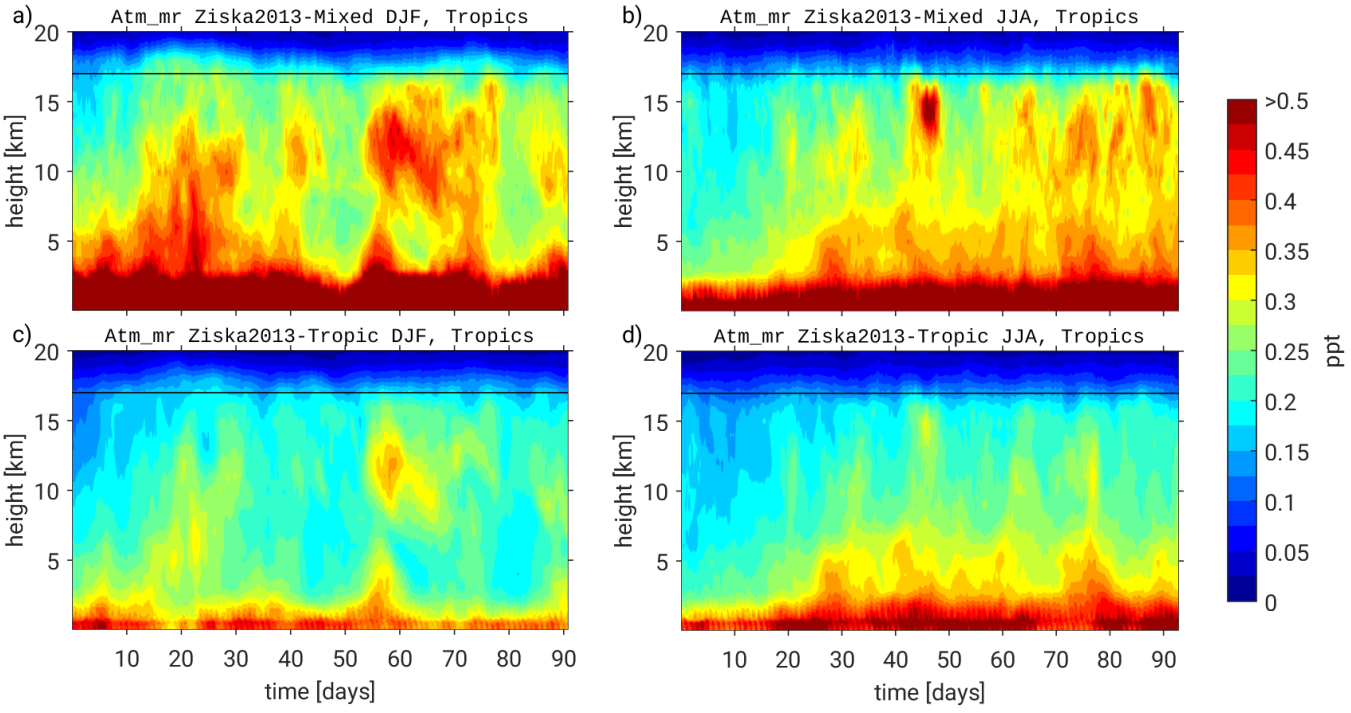

Figure 9: Time series of bromoform mixing ratio [ppt] in the tropics (10° S–20° N, 90° E–120° E) for a) and b) the Ziska2013-Mixed run and c) and d) Ziska2013-Tropics run for both DJF (left) and JJA (right). The black line marks the approximate location of the cold point tropopause at 17 km.

https://doi.org/10.5194/acp-2019-1004
Preprint. Discussion started: 27 January 2020

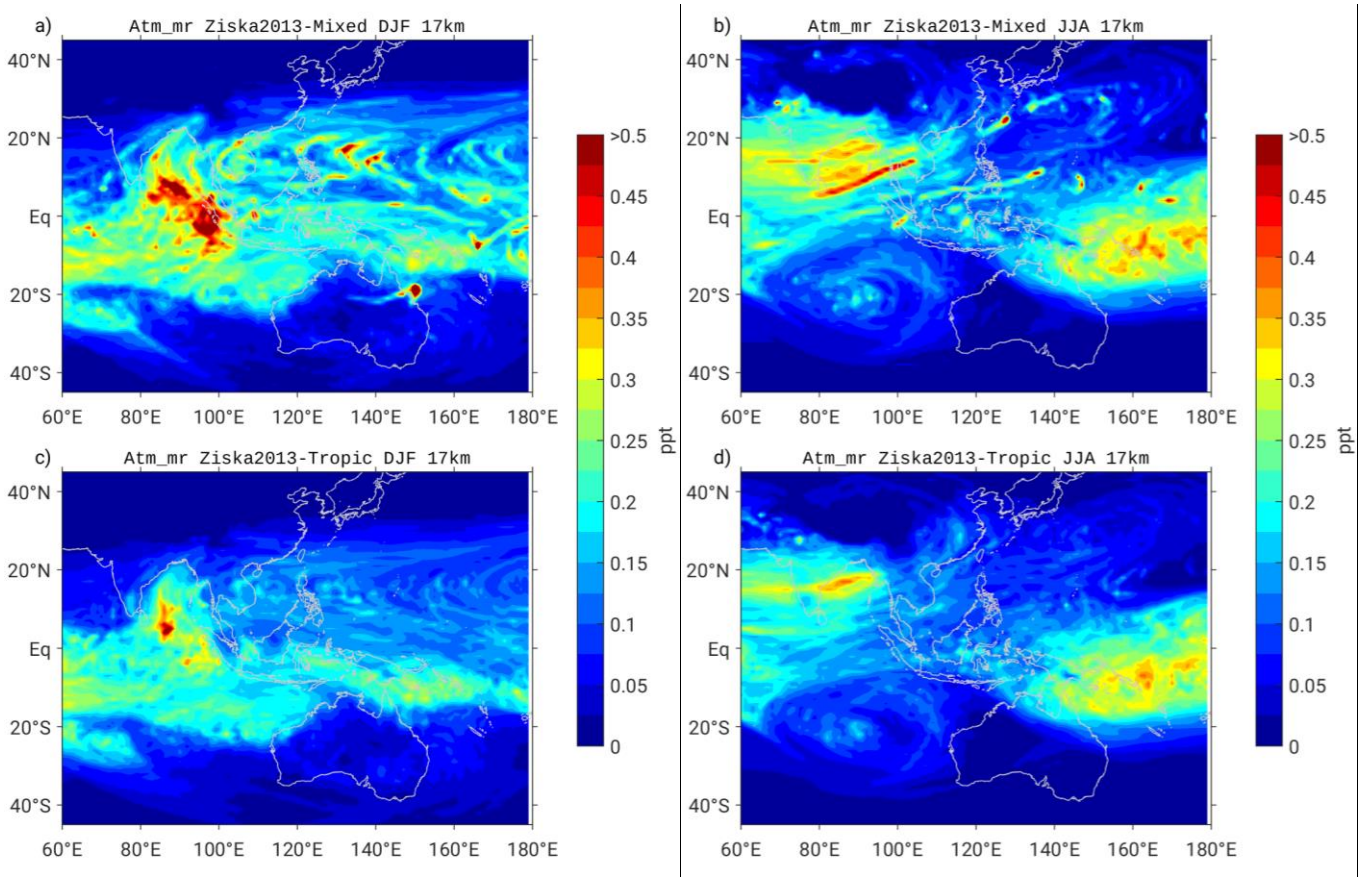

Figure 10: 5-day mean atmospheric mixing ratios [ppt] for a) and b) the Ziska2013-Mixed and c) and d) Ziska2013-Tropics simulation at 17 km height for DJF (left) and JJA (right).